HHS Public Access

Author manuscript

J Med Chem. Author manuscript; available in PMC 2023 February 13.

Published in final edited form as:

J Med Chem. 2021 May 27; 64(10): 6621–6633. doi:10.1021/acs.jmedchem.0c01971.

Adamantyl isothiocyanates as mutant p53 rescuing agents and their structure-activity relationships

Vladimir Burmistrov[1,2,*], **Rahul Saxena**[3], **Dmitry Pitushkin**[1], **Gennady M. Butov**[1,2], **Fung-Lung Chung**[4], **Monika Aggarwal**[4,*,#]

[1]Volgograd State Technical University, Volgograd, 400005, Russia

[2]Department of Chemistry, Technology and Equipment of Chemical Industry, Volzhsky Polytechnic Institute (branch) Volgograd State Technical University, Volzhsky, 404121, Russia

[3]Department of Biochemistry and Molecular and Cellular Biology, Georgetown University, Washington, DC 20007, USA

[4]Department of Oncology, Lombardi Comprehensive Cancer Center, Georgetown University, Washington DC 20007, USA

Abstract

Mutant p53 rescue by small molecules is a promising therapeutic strategy. In this structure-activity relationships study, we examined a series of adamantyl isothiocyanates (Ad-ITCs) to discover novel agents as therapeutics by targeting mutant p53. We demonstrated that the alkyl chain connecting adamantane and ITC is a crucial determinant for Ad-ITC inhibitory potency. Ad-ITC **6** with the longest chain between ITC and adamantane displayed the maximum growth inhibition in $p53^{R280K}$, $p53^{R273H}$, or $p53^{R306Stop}$ mutant cells. Ad-ITC **6** acted in a mutant p53-dependent manner. It rescued $p53^{R280K}$ and $p53^{R273H}$ mutants, thereby, resulting in upregulating canonical wild-type (WT) p53 targets and phosphorylating ATM. Ad-ISeC **14** with selenium showed a significantly enhanced inhibitory potency, without affecting its ability to rescue mutant p53. Ad-ITCs selectively depleted mutant p53, but not the WT, and this activity correlates with their inhibitory potencies. These data suggest Ad-ITCs may serve as novel promising leads for the p53-targeted drug development.

Graphical Abstract

[#]**Correspondence:** Monika Aggarwal, Ph.D, Department of Oncology, Lombardi Comprehensive Cancer Center, Georgetown University, Washington DC 20007, USA, Phone: 202-687-3648; Fax: 202-687-1068; ma1274@georgetown.edu.

[*]These authors contributed equally to this work

Author Contributions: MA contributed to the conception and design of the study, acquisition of experimental data, to the analysis and interpretation of results and to the writing of the manuscript and supervised the study. VB contributed to the acquisition of experimental data, to the analysis and interpretation of results and to the writing of the manuscript. RS contributed to the acquisition of experimental data. FLC provided guidance and encouragement and contributed to the interpretation of results and writing of the manuscript. DP contributed to the synthesis of Ad-ITCs. GMB provided guidance for the synthetic part and contributed to the interpretation of spectral data. All authors read and approved the final manuscript.

Competing Interests statement: The authors declare that they have no competing interests.

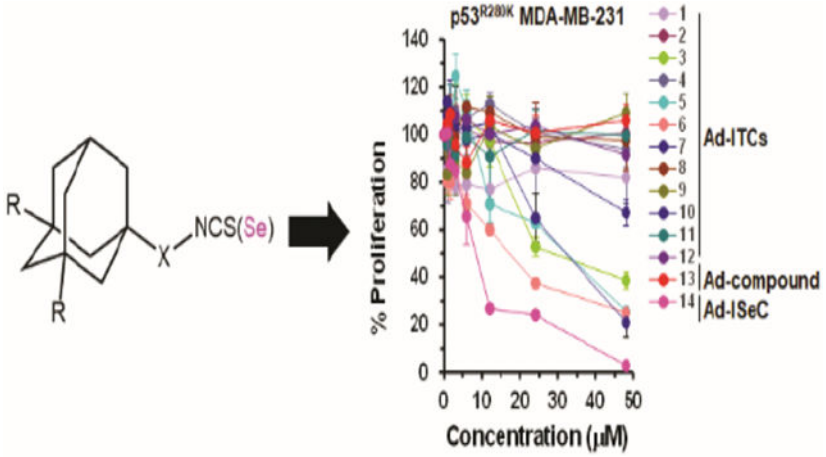

Introduction

Adamantane, a polycyclic cage compound with high symmetry, was originally discovered to display potent antiviral activities. Drugs incorporating adamantane (amantadine, rimantadine, tromantadine, memantine) used for the treatment of viral diseases (Influenza A, herpes) and neurological disorders (Parkinson, Alzheimer) were the first to be introduced to clinics. Adamantane derivatives are used in medicinal chemistry and drug development because of their lipophilic nature that allows modifying various pharmacophores to enhance drug lipophilicity and metabolic stability, thereby improving their pharmacokinetics[1-4]. Adamantane also leads to the better understanding of underlying molecular mechanisms, for example the interactions of aminoadamantane anti-Influenza A agents with the M_2 ion channel[5].

Adamantane derivatives have been studied as promising anti-cancer agents. The cisplatin analog LA-12 that contains the hydrophobic 1-adamantylamine showed cytotoxicity against cisplatin resistant cancers[6-8]. Increased activity of this compound can be attributed to its enhanced ability to penetrate cell membrane[9]. Thus, adamantane scaffolds enhance the metabolic stability, pharmacokinetics, and membrane transfer of the modified drugs[10-12]. Studies of how adamantane scaffolds affect the anti-cancer activities of dietary-related natural compounds, such as isothiocyanates (ITCs), however, are scarce.

ITCs, compounds derived from cruciferous vegetables, inhibit tumorigenesis in animal models[13,14]. Epidemiological studies also support their role in protection against human cancers[15]. Phenethyl isothiocyanate (PEITC), an arylalkyl ITC abundant in watercress, has been investigated under clinical phase 1 and phase 2 trials (http://www.clinicaltrials.gov/ct2/results?term=PEITC). Several activities have been proposed for PEITC, including modulation of phase I and phase II enzymes, oxidative stress, binding to target proteins, cell cycle arrest, and apoptosis[13-20]. We reported that PEITC selectively depletes p53 mutant protein, but not the wild-type (WT), in human cancer cells[21]. These observations led to our recent discovery of a novel mechanism for PEITC in which it reactivates a structural mutant $p53^{R175H}$, *in vitro* and in a breast xenograft mouse model, resulting in tumor growth inhibition[22]. We further demonstrated that PEITC inhibits the growth of prostate cancer cells

expressing p53 structural ($p53^{R175H}$, $p53^{P223L}$) and contact ($p53^{R248W}$) mutants *in vitro* and *in vivo* via mutant p53 rescue[23]. These studies showed for the first time that the anti-cancer activity of PEITC is cancer type-independent, but mutant p53-dependent, suggesting its potential as a "basket trial" agent for cancers harboring mutant p53.

The structure-activity-relationships (SARs) of arylalkyl ITCs to deplete mutant p53 and to induce apoptosis[21] were previously studied in human cancer cells. These studies revealed that increased lipophilicity by incorporating aromatic rings is one of the key structural features important for their increased potency[21]. Here, we describe a study in which the effects of combining an ITC group with a highly lipophilic and metabolically inert cycloalkane adamantane, adamantyl-ITCs (Ad-ITCs), on its anti-cancer activities are investigated. We evaluated the activities of Ad-ITCs as potential novel cancer therapeutics by targeting mutant p53 in triple negative breast cancer (TNBC) cells and its SARs. TNBC are an aggressive subset of breast cancer that are not amenable to endocrine therapy due to the lack of estrogen receptor (ER) /progesterone receptor (PR) and human epidermal growth factor receptor 2 (HER2) and they often show resistance to current chemotherapeutic agents. TNBC displays a highest frequency of p53 gene mutation (~80%) among the different subtypes of breast cancers[24,25]. In fact, p53 is the most frequently mutated gene in TNBC, suggesting its crucial role in this disease[26]. Despite this, therapeutic options targeting mutant p53 in TNBC patients are lacking.

Results

Effects of Ad-ITCs on $p53^{R280K}$ MDA-MB-231 cells proliferation

We examined a series of ITCs containing an adamantyl moiety, Ad-ITCs **1**-**12** (Figures 1 and S1-4), that were synthesized as described previously[27], except compounds **6** and **8** that were synthesized in this study. Ad-ITCs **1** and **2** are structures with a —N═C═S in nodal and bridge positions of adamantane. Ad-ITCs **3**, **5**, and **6** have an aliphatic bridge of 1-3 carbon atoms and Ad-ITC **7** have an aromatic bridge between —N═C═S and adamantane. These compounds should determine how the bridge length connecting adamantane and ITC and the substituents on it influences their activities. Ad-ITCs **4** and **10** have branched aliphatic chains between —N═C═S and adamantane. They should reveal how steric hindrance affects the activities. Ad-ITCs **8**, **9**, and **12** containing oxygen atom in the alkyl chain allow to evaluate the effects of the electron withdrawing by the oxygen atom near ITC group. Finally, Ad-ITC **11** with two methyl groups on the adamantane is expected to further enhance lipophilicity resulting in even better absorption by tissues, such as blood-brain barrier.

Ad-ITCs **1**-**11** were synthesized from the corresponding amines by a two-step reaction (Figure S1A,B)[27]. The amines were first reacted with CS_2 in ethanol in presence of Et_3N. The formation of Et_3N salt of corresponding carbamodithioic acid occurs at room temperature (RT) within 30 minutes. Next, BoC_2O and a catalytic amount of DMAP were added at 0°C. The desulfurization led to formation of compounds **1**-**11**. Ad-ITC **12** was synthesized by treating adamantyl acetic acid chloride with sodium thiocyanate (Fig. S1C).

To study whether —N═C═S group is essential for its activity, Ad-compound **13** was used[28]. Ad-compound **13** is a 2-thioxoimidazolidin-4-one derivative prepared from Ad-ITC **5** (Figure S1D). It retains the structure of Ad-ITC **5** except that the ITC group is replaced by a thiooxoimidazole ring. Octanol/Water partition coefficients were also measured for compounds **1**-**13** (Table S1). Log *P* for Ad-ITC **1**-**12** were within the range of 3.73-6.77. Except for the two most lipophilic compounds, Ad-ITC **7** (log *P* 6.34) and Ad-ITC **10** (log *P* 6.77) and the least lipophilic Ad-ITC **12** (log *P* 3.73), the lipophilicity of Ad-ITCs was relatively consistent (log *P* 5.0 ± 0.5). These values satisfy the Lipinski's rule of five[29]. Such lipophilicity is favorable for the transport of molecules through the cell membrane and for protein binding as observed previously for adamantane containing drugs[30,31].

To determine the biological activity and the structural features important for the activity, we divided Ad-ITCs into four categories: (1) Ad-ITCs with different alkyl chain length connecting the adamantane to ITC (**1**, **2**, **3**, **5**, **6**), (2) Ad-ITCs with electron releasing substituents, electron withdrawing substituents, branched chains, double bonds, or heteroatoms in the alkyl chain (**4**, **8**, **9**, **10**, **12**), (3) the Ad-ITC with a benzene ring between adamantane and ITC (**7**), and (4) Ad-ITC **11** with electron releasing alkyl substituents on adamantane. The proliferation of $p53^{R280K}$ MDA-MB-231 TNBC cells treated with various concentrations of Ad-ITCs **1**-**12** or Ad-compound **13** for 24 h or 72 h was compared with dimethyl sulfoxide (DMSO)-treated cells (as a control). Of all the 13 compounds tested, only **3**, **5**, **6**, and **7** displayed dose-dependent activity (Figure 2A).

Ad-ITC **6** with the three carbon alkyl chain connecting the ITC to adamantane showed the greatest inhibition against MDA-MB-231 cell proliferation (IC_{50} between 12-24 μM) followed by Ad-ITCs **5** and **3** (two and one carbon alkyl chain, respectively) (IC_{50} between 24-48 μM) after 24 h (Figure 2A). After 72 h, both Ad-ITCs **5** and **6** displayed IC_{50} between 12-24 μM, whereas, for Ad-ITC **3** ~50% inhibition of cell proliferation remained between 24-48 μM (Figure S5A). Consistent with this finding, the Ad-ITCs containing a bulky adamantane adjacent to ITC (**1, 2,** and **11)** that are likely to cause steric hindrance, therefore, blocking their binding to the target proteins, failed to show any significant inhibition of cell proliferation (Figures 2A and S5A). Ad-ITC **7** showed enhanced potency when compared with Ad-ITCs **1** and **2** (Figures 2A and S5A), however, this compound was significantly less potent than Ad-ITCs **3**, **5**, and **6**. The lower potency of Ad-ITC **7** could be due to an aromatic ring adjacent to the —N═C═S leading to low mobility and the inability to adjust to the active site.

The Ad-ITCs **4** and **10** with branched alkyl chains did not show any significant inhibition of MDA-MB-231 cells proliferation (Figures 2A and S5A). These data could reflect a weaker binding to the target protein due to steric hindrance created by the alkyl substitution adjacent to the ITC. Ad-ITC **12** with a double bond failed to inhibit the cell proliferation (Figures 2A and S5A). Similarly, Ad-ITCs **8** and **9** with an oxygen atom replacing gamma-carbon were not active *in vitro* (Figures 2A and S5A), suggesting that the addition of heteroatom could lead to the loss of activity. Importantly, Ad-compound **13** that lacked ITC group did not inhibit the proliferation of MDA-MB-231 cells, suggesting that the ITC group is essential for the biological activity of Ad-ITCs (Figures 2A and S5A). We also examined

the effects of pure adamantane on MDA-MB-231 cell proliferation. Our results showed that adamantane did not inhibit MDA-MB-231 cells proliferation (Figures S6), thus confirming that —N═C═S functional group is required for the activity of Ad-ITCs. Previously, we have shown that PEITC inhibits the growth of cancer cells expressing mutant p53[22,23]. As a positive control we also examined the effects of PEITC on the proliferation of MDA-MB-231 cells (Figures S6). Collectively, these results demonstrated that the potency of Ad-ITC to inhibit MDA-MB-231 cell proliferation enhances with increasing the length of aliphatic alkyl chain connecting ITC to adamantane and decreases with the introduction of substituents, possibly due to steric hindrance at the α-position to the ITC.

Effects of Ad-ITCs on proliferation of $p53^{R273H}$ MDA-MB-468 and WT p53 MCF-7 cells

To validate that increase in the length of aliphatic alkyl chain connecting adamantane to ITC enhances the potency of Ad-ITCs to inhibit cell proliferation, we evaluated the effects of Ad-ITCs **3**, **5**, and **6** on a different p53 mutant TNBC cell line MDA-MB-468 ($p53^{R273H}$). Consistent with our findings with MDA-MB-231 cells, Ad-ITC **6** showed the greatest inhibition of $p53^{R273H}$ MDA-MB-468 cells proliferation at 24 h and 72 h (IC_{50} between 12-24 μM) (Figures 2B and S5B). As expected, Ad-compound **13** (Figures 2B and S5B) and adamantane (Figure S6) did not inhibit MDA-MB-468 cells proliferation. As a positive control, we also examined the effects of PEITC on the proliferation of MDA-MB-468 cells (Figure S6). Thus, the length of aliphatic alkyl chain is a crucial determinant of Ad-ITC potential to inhibit cell proliferation. These results agree with our previous observations that the potency of aromatic ITC enhanced with increase in alkyl chain length[21,32].

We evaluated the effects of Ad-ITCs **3**, **5**, and **6** on proliferation of WT p53 MCF-7 cells. MCF-7 cells were remarkably less sensitive to Ad-ITCs **3** and **6** when compared to $p53^{R280K}$ MDA-MB-231 and $p53^{R273H}$ MDA-MB-468 cells (Figures 2C and S5C). Consistent with this, MCF-7 cells were also considerably less sensitive to PEITC that was used as a positive control in these experiments (Figure S6). Ad-ITC **5** and Ad-compound **13** (Figures 2C and S5C) and adamantane (Figure S6) did not inhibit MCF-7 cell proliferation. These results demonstrated that $p53^{R280K}$ MDA-MB-231 and $p53^{R273H}$ MDA-MB-468 are significantly more sensitive to Ad-ITCs **3** and **6** than the WT p53 MCF-7 cells.

Colony formation assays to determine the effects of Ad-ITCs on proliferation of $p53^{R280K}$ MDA-MB-231 and WT p53 MCF-7 cells

We performed colony formation assay (CFA) with selected compounds with differential abilities to inhibit cell proliferation, **1** (mild inhibition), **6** (maximum inhibition), and **13** (as a negative control). Similar differences in the sensitivities of $p53^{R280K}$ MDA-MB-231 and WT p53 MCF-7 cells to Ad-ITC **6** were observed in CFA (Figure S7). These data reinforce the findings that mutant p53 cells are more sensitive to growth inhibition by Ad-ITC **6** compared to the WT p53 cells.

Ad-ITCs induce apoptosis in mutant p53 TNBC cells

The inhibitory effects of Ad-ITCs **3**, **5**, and **6** on cell proliferation suggested that these compounds might also possess apoptotic potential. The $p53^{R280K}$ MDA-MB-231 and $p53^{R273H}$ MDA-MB-468 cells treated with 6 μM or 12 μM of Ad-ITCs **3**, **5**, or **6** showed

a significant (~2.0-5.1-fold) increase in the Annexin V stained cells as compared to the DMSO-treated cells (Figure 3A,B and S8A). Ad-ITC **1** and Ad-compound **13** (6 μM or 12 μM), used as negative controls, did not induce significant increase in apoptosis of MDA-MB-231 and MDA-MB-468 cells (Figure 3A,B). WT p53 MCF-7 cells treated with Ad-ITCs **1**, **3**, **5**, **6** or Ad-compound **13** did not display any significant increase in Annexin-V-stained cells (Figure 3C and S8A). As a positive control, we also examined the effects of PEITC on induction of apoptosis in $p53^{R280K}$ MDA-MB-231, $p53^{R273H}$ MDA-MB-468, and WT p53 MCF-7 cells (Figure S9A and B).

Cleavage of poly(ADP-ribose) polymerase-1 (PARP1) by caspase 3 is considered to be the hallmark of apoptosis[33]. Therefore, to further confirm the apoptotic potential of Ad-ITCs, we examined the effects of most potent compound Ad-ITC **6** on caspase 3 and PARP1 levels in $p53^{R280K}$ MDA-MB-231, $p53^{R273H}$ MDA-MB-468, and WT p53 MCF-7 cells. Western blot analysis showed a significant decrease in the levels of uncleaved caspase 3 and PARP1 in $p53^{R280K}$ MDA-MB-231 and $p53^{R273H}$ MDA-MB-468 cells treated with 6 μM or 1 μM of Ad-ITC **6** (Figure S8B). We also detected a concomitant increase in the levels of cleaved-PARP1 in these cells (Figure S8B). Consistent with the Annexin V results (Figures 3C), we did not detect any significant decrease in the levels of uncleaved PARP1 or accumulation of cleaved-PARP1 fragments in WT p53 MCF-7 cells (Figure S8B). MCF-7 cells are deficient in caspase 3[34]. Therefore, we did not detect any caspase 3 expression in WT p53 MCF-7 cells (Figure S8B). PEITC treated $p53^{R280K}$ MDA-MB-231 and $p53^{R273H}$ MDA-MB-468 cells, used as a positive control, also displayed a significant decrease in the levels of uncleaved caspase 3 and accumulation of cleaved-PARP1 fragments (Figure S9C). However, we observed a significant decrease in the levels of uncleaved PARP1 and accumulation of cleaved-PARP1 in PEITC treated caspase 3-deficient MCF-7 cells (Figure S9C). These results are consistent with the previous reports[33,34], that suggest a possible involvement of other caspases in the cleavage of PARP1 in the absence of caspase 3. These results further support that mutant p53 cells were more sensitive to Ad-ITCs with specific structural features.

Effects of Ad-ITCs on the expression of p53 protein

Since aromatic ITCs can selectively deplete mutant p53 protein[21], we examined the effects of Ad-ITCs **3**, **5** and **6** on p53 expression in mutant p53 cells. Treatment with Ad-ITCs (6 μM or 12 μM) for 24 h led to a differential decrease in the expression of mutant p53 in MDA-MB-231 and MDA-MB-468 cells (Figure 3D). As expected, no depletion was observed with Ad-ITC **1** in both the cell lines (Figure 3D). These results demonstrated that the ability of Ad-ITCs to reduce mutant p53 expression seems to correlate with their growth inhibitory potencies. Concurrently, the alkyl chain length seems to influence their potency in reducing the expression of mutant p53. Furthermore, ITC group is essential for this activity as Ad-compound **13** failed to affect mutant p53 expression. On the contrary, Ad-ITCs **1**, **3**, **5**, **6** and Ad-compound **13** did not decrease WT p53 expression in MCF-7 cells (Figure 3D). As a positive control, we also examined the effects of PEITC on p53 expression levels in MDA-MB-231, MDA-MB-468, and MCF-7 cells (Figure S9C). We observed a significant decrease in the expression of $p53^{R280K}$ and $p53^{R273H}$ mutants in PEITC (6 μM or 12 μM) treated MDA-MB-231 and MDA-MB-468 cells, respectively. Consistent with our previous

study[21], we also detected an increase in p53 levels in MCF-7 cells (Figure S9C). These results suggest that mutant p53 is an important target for these novel Ad-ITCs.

Ad-ITC 6 rescues p53 mutants and activates Ataxia-Telangiectasia Mutated (ATM)

Since Ad-ITC **6** induced apoptosis in mutant p53 cells, we reasoned it may do so by restoring WT functions. Therefore, we determined its effects on the canonical p53 targets in these cells. Treatment with 6 μM Ad-ITC **6** enhanced the expression of the canonical p53 targets p21 and NOXA in both MDA-MB-231 and MDA-MB-468 cells (Figure 4A). These results suggested that Ad-ITC **6** restores transactivation functions to $p53^{R280K}$ and $p53^{R273H}$ mutants in MDA-MB-231 and MDA-MB-468 cells, respectively. Ad-ITC **6** also upregulated expression of p21 and NOXA in WT p53 MCF-7 cells (Figure 4A). The WT p53 is regulated by MDM2 by an autoregulatory feedback loop[35]. Consistent with this idea, 6 μM Ad-ITC **6** enhanced the expression of MDM2 in both $p53^{R273H}$ MDA-MB-468 and WT p53 MCF-7 cells (Figure S10A). These results demonstrated that Ad-ITC **6** can not only rescue mutant p53, but also activates WT p53.

To determine whether depletion of mutant p53 in cells occurs at the transcriptional or post-transcriptional level, we compared the mRNA levels of p53 in DMSO and Ad-ITC **6** treated MDA-MB-231 and MDA-MB-468 cells. As a control, we also evaluated mRNA levels of p53 in WT p53 MCF-7 cells. As shown in Figure S10B, 4 h after Ad-ITC **6** treatment, the mutant p53 mRNA levels remained unchanged in MDA-MB-231 and MDA-MB-468 cells. Therefore, Ad-ITC **6** depleted mutant p53 without causing changes in the p53 mRNA expression levels. These results strongly suggest that Ad-ITC **6** depletes mutant p53 at the post-transcriptional level. These findings are consistent with our previous studies where we have shown that PEITC depletes mutant p53 at post-transcriptional level[21]. We also detected an increase in the p53 mRNA level in MCF-7 cells (Figure S10B); however, we did not observe any significant increase in the WT p53 protein (Figure 3D).

WT p53 plays a crucial role in cell cycle progression and genome stability maintenance by inducing DNA damage response (DDR) pathway. We examined if the reactivated $p53^{R280K}$ and $p53^{R273H}$ mutants could modulate cell cycle progression. $p53^{R280K}$ MDA-MB-231 and $p53^{R273H}$ MDA-MB-468 cells treated with Ad-ITC **6** (6 μM) displayed a significant delay in G1 phase compared to DMSO-treated cells at 24 h (48.2% and 53.23% vs. 42.9% and 30.6%, respectively) (Figure 4B). WT p53 MCF-7 cells treated with Ad-ITC **6** (6 μM) display a small increase in G2/M phase compared with DMSO-treated cells (24.3% vs 21.3%) (Figure 4B). These results confirmed that Ad-ITC **6** restores “WT-like” functions to $p53^{R280K}$ and $p53^{R273H}$ mutants in TNBC cells.

We examined if the delay in cell cycle progression was due to activation of DDR pathway. As a gain of function (GOF) activity mutant p53 inhibits activation of ATM by impairing its recruitment to the site of DNA damage and induces genetic instability[36]. Previously, we showed that PEITC induced rescue of mutant p53 abolished this GOF activity[22,23]. Here, we showed that treatment with 6 μM Ad-ITC **6** resulted in phosphorylation of ATM at S1981 in MDA-MB-231 and MDA-MB-468 cells (Figure 4C), suggesting that restoration of WT p53 functions to $p53^{R280K}$ and $p53^{R273H}$ mutants abolishes their ability to inhibit the activation

of ATM. Consistent with the WT p53 expression level (Figure 3D) and cell cycle data (Figure 4B), pATM-S1981 was absent in WT p53 MCF-7 cells (Figure 4C). Taken together, these results suggest that Ad-ITC **6** rescues $p53^{R280K}$ or $p53^{R273H}$ and reactivates DDR.

Ad-ITC 6 inhibits cell proliferation via mutant p53

To determine if the anti-proliferative effects of Ad-ITC **6** were mediated through mutant p53, we examined its effects on the proliferation of p53 null MDA-MB-436 cells. MDA-MB-436 cells treated with Ad-ITC **6** showed significantly reduced sensitivity at 24 h and 72 h (Figure 5A,B) compared to the $p53^{R280K}$ MDA-MB-231 or $p53^{R273H}$ MDA-MB-468 cells (Figures 2A,B and S5A,B). To further confirm the mutant p53 mediated inhibition of cell proliferation, we compared Ad-ITC **6** effects on MDA-MB-468 cells that were transfected either with p53 siRNA or non-specific (NS) siRNA. The p53 knockdown MDA-MB-468 cells showed markedly reduced sensitivity to Ad-ITC **6**, whereas NS siRNA MDA-MB-468 cells remained highly sensitive (Figure S11). These results showed that Ad-ITC **6** induced inhibition of cell proliferation is, at least partially, dependent on mutant p53.

We also examined the anti-proliferative effects of Ad-ITC **6** on a TNBC cell line HCC1937 that express a truncated $p53^{R306Stop}$ mutant. HCC1937 cells displayed a remarkable sensitivity to Ad-ITC **6** (IC_{50} = 12 μM) (Figure 5A,B). These results strongly demonstrated the functional involvement of the mutational status of p53 in cell response to Ad-ITC **6**.

Ad-ISeC 14 displayed enhance potency compared to Ad-ITCs

Since —N═C═S group is essential for the activity of Ad-ITCs, we determined if replacing the sulfur (S) in the ITC with selenium (Se) will influence its activities. The Se atom was selected as it exhibits cancer chemopreventive activities and is an integral part of many mammalian selenoproteins that may influence various pathways of cancer development[37,38]. We used an analog of Ad-ITC **5** where S in the ITC has been substituted with a Se, 1-isoselenocyanato-2-(adamantan-1-yl)ethane (Ad-ISeC **14**) (Figure S12A and B)[30]. Octanol/Water partition coefficients was measured for Ad-ISeC **14** (Table S1). Most of the known methods of Ad-ISeC synthesis use potassium selenocyanate that spontaneously convert to potassium cyanate even at 4°C. Isocyanates have high reactivity, water sensibility and toxicity. We adapted a relatively easy and safe method for the synthesis of isoselenocyanates, including 1-isoselenocyanatoadamantane[39].

Ad-ISeC **14** (Figure 6A) displayed the maximum potency to inhibit proliferation of $p53^{R280K}$ MDA-MB-231 or $p53^{R273H}$ MDA-MB-468 cells at 24 h and 72 h (IC_{50} between 6 μM and 12 μM, respectively) (Figures 6B and S12C) when compared to all S containing Ad-ITCs, including Ad-ITC **5** (Figures 2A,B and S5A,B). These results demonstrated that the substitution of S with Se in Ad-ITC **5** enhanced its potency, presumably because of its electron-withdrawing property rendering it more electrophilic. Such substitution also enhances water solubility (LogP of Ad-ISeC **14** is 4.05 which is 0.71 points lower than of Ad-ITC **5**). Ad-ISeC **14** also inhibited MCF7 cell proliferation, however, these cells were considerably less sensitive than mutant p53 cells (Figures 6B and S12C). Similar differences in the sensitivities of MDA-MB-231 and MCF-7 cells to Ad-ISeC **14** were also observed in

CFA (Figure S12D). These results demonstrated that the p53 mutation status in TNBC cells plays an important role in sensitizing cells to Ad-ISeC **14**.

Treatment with Ad-ISeC **14** (6 μM or 12 μM) enhanced the apoptotic potential of MDA-MB-231 and MDA-MB-468 cells but not in MCF-7 cells (Figure 6C and S13A). In fact, Ad-ISeC **14** (6 μM or 12 μM) induced a significantly greater (>2-fold) level of apoptosis in $p53^{R273H}$ MDA-MB-468 cells when compared to Ad-ITC **5** (6 μM or 12 μM) (Figure 3B). To further confirm the apoptotic potential of Ad-ISeC **14**, we demonstrated a decrease in the levels of uncleaved caspase 3 and PARP-1 and an increase in the levels of cleaved-PARP1 fragment in Ad-ISeC **14** treated MDA-MB-231 and MDA-MB-468 cells (Figure S13B). We did not detect any significant change in the levels of uncleaved PARP1, uncleaved caspase 3, or accumulation of cleaved-PARP1 in MCF7 cells (Figure S13B). MDA-MB-231 and MDA-MB-468 cells treated with Ad-ISeC **14** (6 μM or 12 μM) showed a significant reduction in mutant p53 expression when compared to the DMSO control (Figure 6D). Ad-ISeC **14** (6 μM or 12 μM) induced a significantly greater decrease in the $p53^{R280K}$ and $p53^{R273H}$ expression levels in MDA-MB-231 and MDA-MB-468 cells, respectively, when compared to Ad-ITC **5** (6 μM or 12 μM) (Figure 3C). Together, like its sulfur counterpart, these results showed a correlation between the growth inhibitory potency and the ability to destabilize mutant p53 in TNBC cells, suggesting that Se does not influence Ad-ISeC **14** interactions with the target proteins. Contrary to mutant p53, WT p53 expression appeared marginally elevated after treatment with 12 μM Ad-ISeC **14** (Figure 6D), suggesting that Ad-ISeC **14** might activate WT p53. Ad-ISeC **14** (6 μM) significantly enhanced the levels of p21 and NOXA in MDA-MB-231 and MDA-MB-468 cells (Figure 6E), demonstrating that it restored the transactivational functions to $p53^{R280K}$ and $p53^{R273H}$ mutants. A significant increase in the expression levels was also observed in the MCF-7 treated with 6 μM Ad-ISeC **14** (Figure 6E), suggesting that Ad-ISeC **14** also activated WT p53. We also detected a statistically significant elevation of MDM2 in both $p53^{R273H}$ MDA-MB-468 and WT p53 MCF-7 cells (Figure S14A). Taken together, these data strongly suggest that Ad-ISeC **14** can not only reactivates mutant p53, but also activate WT p53.

To determine whether Ad-ISeC **14** also depletes mutant p53 at post-transcriptional level, we examined the mRNA levels of p53 in DMSO and Ad-ISeC **14** treated MDA-MB-231 and MDA-MB-468 cells. As shown in Figure S14B, the mutant p53 mRNA levels remained unchanged in MDA-MB-231 and MDA-MB-468 cells after Ad-ISeC **14** treatment. These results strongly suggest that Ad-ISeC **14** depletes mutant p53 at the post-transcriptional level. We also detected an increase in the p53 mRNA level in MCF-7 cells treated with Ad-ISeC **14** (Figure S14B). Consistent with this, we also detected an elevated levels of WT p53 in Ad-ISeC **14** treated MCF-7 cells (Figure 6D).

Effects of Ad-ITC 6 and Ad-ISeC 14 on proliferation of normal cells

To determine if Ad-ITC **6** and Ad-ISeC **14** have inhibitory effects on the proliferation of normal cells, we examined their effects on two different normal cell types, mammary epithelial cells (MCF10A) and colon cells (CCD841), expressing WT p53. Our results showed that IC_{50} for Ad-ITC **6** and Ad-ISeC **14** were significantly higher than the $p53^{R280K}$ MDA-MB-231 and $p53^{R273H}$ MDA-MB-468 tumor cells (Figure S15). These

results further support that Ad-ITCs may serve as novel promising leads for p53-targeted drug development.

Discussion and Conclusions

The p53 gene is most frequently mutated gene in human cancers. These mutations are predominantly missense (~74%) and are classified as either structural (e.g., R175H) or contact (e.g., R273H). Mutations in p53 impair WT activity; however, the mutants may also gain oncogenic functions[40,41]. Small molecules that can rescue mutant p53 have been identified and are now under clinical investigations[25,42,43]. However, studies to investigate the potential of small molecules towards targeting mutant p53 in TNBC are limited. In this study we showed that, depending on their structures, the novel Ad-ITCs **3**, **5**, **6** and Ad-ISeC **14** exhibited potential anti-cancer activities against $p53^{R280K}$ and $p53^{R273H}$ mutant TNBC cells. These compounds also inhibited the proliferation of WT p53 MCF-7 cells; albeit the mutant p53 cells were more sensitive. Ad-ITC **6** and Ad-ISeC **14** induced apoptosis selectively in mutant p53 cells, and not in WT p53, as evidenced by Annexin V staining and western blot analysis of caspase 3 and PARP1 cleavage. Supporting mutant p53 as a target, Ad-ITC **6** and Ad-ISeC **14** selectively depleted mutant p53 protein, but not WT, in these cells.

The SARs revealed the importance of the alkyl chain length connecting adamantane and —N═C═S in Ad-ITCs anti-cancer activities. Elongation of the alkyl chain from 0 to 3 carbons significantly enhance the antiproliferative potency of Ad-ITCs, following an order of Ad-ITC **6**>**5**>**3**>**1**. Concurrently, the alkyl chain length markedly affects its mutant p53 depleting activity. The greater potency for longer alkyl chain Ad-ITCs may reflect the diminished steric hindrance and an increase lipophilicity as evidenced by their logP values. Both structural features are favorable for interactions with the target proteins. Previously, we showed that enhanced inhibitory potential of aromatic ITCs with an increase in alkyl chain length and lipophilicity of the side chain moiety *in vitro* and in a mouse model of lung tumorigenesis[21,32].

The lack of anti-proliferative activity for Ad-ITC **8**, an analog of Ad-ITC **6**, where carbon atom of the bridge closest to adamantane was substituted by oxygen atom, could be attributed to its lower lipophilicity as compared to Ad-ITC **6** (logP values 4.42 vs 5.17, respectively) and altered electron distribution characteristics. These hypotheses may be further examined by synthesizing Ad-ITCs containing different hydrogen bond acceptors and hydrogen bond donors such as F, Cl, OH, O-CH_3 etc. in nodal and bridge positions of adamantyl along with a linker between adamantane and ITC.

A comparison of the IC_{50} of Ad-ITC **5** with PEITC demonstrates the differential effects of an aryl vs. an adamantyl group on the activities of ITCs. Because Ad-ITC **5** is more lipophilic than PEITC (logP values 4.76 vs 3.50, respectively), we expected lower IC_{50} for Ad-ITC **5** and its longer chain analogs than PEITC[22,23]. This suggests that other factors could also affect the potency of Ad-ITCs, including their size, shape, and the resulting rigidity. Thus, it is possible that a longer alkyl chain length in Ad-ITCs may lead to IC_{50} comparable to or even better than that of the corresponding aromatic ITCs.

Similar to ITCs, the chemopreventive effects of ISeC may be attributed to redox modulation and modification of protein thiols and ISeC can act synergistically with ITCs[44]. Furthermore, the substitution of S with Se in aromatic ITCs resulted in compounds with lower IC_{50}s[45]. Interestingly, Ad-ISeC **14** displayed a significantly greater anti-proliferative activity compared to S containing analog Ad-ITC **5**. In fact, the IC_{50} for Ad-ISeC **14** was similar to that of PEITC in p53 contact mutant cells[22,23]. Furthermore, Ad-ISeC **14** induced a significantly greater level of apoptosis in $p53^{R273H}$ MDA-MB-468 cells and a decrease in the levels of $p53^{R280K}$ and $p53^{R273H}$ mutants compared to Ad-ITC **5**. Because same starting amine can be used for the synthesis of Ad-ITC **5** and Ad-ISeC **14**, the preparation of ISeCs with longer bridge (up to $(CH_2)_5$) should be readily attainable[46]. The Se-containing compounds with general formula R-Se-R (selenides), R-SeH (selenols), and R-Se-Se-R (diselenides) may be synthesized.

Our results showed that Ad-ITC **6** and Ad-ISeC **14** causes mutant p53 depletion at the post-transcriptional level since the levels of mutant p53 mRNA remains unchanged in Ad-ITC **6** or Ad-ISeC **14** treated MDA-MB-231 and MDA-MB-468 cells. Ad-ITC **6** and Ad-ISeC **14** rescued $p53R^{280K}$ and $p53^{R273H}$ mutants. Ad-ITC **6** caused a G1 phase arrest and pATM-S1981. Consistent with this idea, the reactivation of DDR might be responsible for the activation of rescued p53 mutants and apoptosis. Previously, we showed that PEITC induced oxidative stress activates DDR in the presence of restored p53 mutant[22,23]. The activation of ATM in Ad-ITC **6**-treated cells suggests that these compounds may also exert oxidative stress. The data on Ad-ITCs reinforce a mechanism involving the binding of Ad-ITC to the mutant p53 protein via —N═C═S through hydrophobic interactions. We also detected an upregulation of canonical p53 targets in Ad-ITC **6**-treated MCF-7 cells, but without a significant change in the cell cycle. Supporting this, we did not detect any phosphorylation of ATM. Collectively, these results suggests that the WT p53 cells may respond to Ad-ITCs via a different mechanism. Further studies are needed to understand the divergent mechanisms in WT p53 cells.

The p53 exon-6 truncating nonsense mutations occur at higher than expected frequencies and promote cancer cell proliferation, survival, and metastasis[47]. However, the studies exploring the potential of the truncated p53 mutants in targeted therapies are scarce. We showed that Ad-ITC **6** inhibited the proliferation of HCC1937 cells harboring a truncated $p53^{R306Stop}$ mutant. An in-depth mechanistic study of Ad-ITC **6** on cell lines harboring p53 exon-6 truncating mutations is important to gain insights into the underlying mechanism. These studies may open up avenues to develop strategies to target cancers harboring these prevalent p53 truncating mutations, unlike p53 point mutants that are classified as DNA binding or structural mutants, an area that warrants comprehensive investigation.

The adamantyl moiety is relatively inert to metabolic transformation and highly stable in humans[4,48,49], and compounds containing adamantane are likely to have a better pharmacokinetic profile *in vivo*. In support of this notion, previous pharmacokinetics studies of anti-viral drugs incorporating adamantane[48,49], amantadine, and rimantadine, have demonstrated that these drugs are highly stable in humans with elimination half-life between 24-60 h and a significantly greater steady-state volumes of distribution in human plasma. Previously, we have shown in a phase I safety and pharmacokinetic clinical trial

(NCT00005883) of PEITC, an aromatic ring containing ITC, that the estimated half-life of PEITC is ~2.4 h and four daily doses of PEITC are required to maintain steady state plasma ITC levels throughout the 24 h[50]. These studies clearly indicate that an extensive investigation on adamantane derivatives of ITCs, including Ad-ITC **6,** Ad-ISeC **14**, and other adamantyl containing ITCs/ ISeCs, *in vitro* and *in vivo*, are needed urgently to unravel their mechanisms, pharmacokinetic profiles, and efficacies. Nevertheless, a new insight is afforded by our study that previously unappreciated adamantyl moiety can be added to ITCs that has potential to enhance the lipophilicity and efficacy of an existing anti-cancer agents, thus, laying a platform for the development of adamantyl compounds as novel p53 targeted therapeutic agents.

Experimental Section

Synthesis of Ad-ITCs 1-11.

Carbon disulfide (40-80 mmol) and triethylamine (4-8 mmol) were added to a mixture of corresponding adamantyl amine (4-8 mmol) and 6-12 mL of ethanol. The mixture was stirred for 30 min at RT and cooled to 0°C. Di-*tert*-butyl dicarbonate (BoC_2O, 4-8 mmol) and 4-(dimethylamino)pyridine (DMAP, 0.01-0.02 g) were added, and the mixture was stirred for 1 h at RT. The solvent was distilled off, and the residue was purified either by crystallization from EtOH (for solid compounds) or by column chromatography (for liquid compounds). For details see below and Ref 27. Purity of synthesized compounds were determined via GC-MS (Agilent GC 5975/MSD 7820) and is >95%.

1-Isothiocyanatoadamantane (1).

The general method above was used with 1-aminoadamantane to afford white solid (1.06 g, 92% yield), mp 167°C. MS (EI): m/z (%) = 193 (47) $[M]^+$, 135 (100) $[Ad]^+$. ^1H NMR (400 MHz, $CDCl_3$): δ = 2.01-1.46 (m, 15H). ^{13}C NMR (100 MHz, $CDCl_3$): δ = 129.45 (s, 1C, NCS), 58.54 (s, 1C, quaternary C in Ad), 43.83 (s, 3C, Ad), 35.61 (s, 3C, Ad), 29.29 (s, 3C, Ad). Elemental analysis calculated for $C_{11}H_{15}NS$: C 68.35, H 7.82, N 7.25, S 16.58; found C 68.33, H 7.83, N 7.24, S 16.60.

2-Isothiocyanatoadamantane (2).

The general method above was used with 2-aminomethyladamantane to afford white solid (1.10 g, 86% yield), mp 140-141°C. MS (EI): m/z (%) = 193 (100) $[M]^+$, 135 (100) $[Ad]^+$. ^1H NMR (500 MHz, $CDCl_3$): δ = 3.89 (s, CH-NCS), 2.12-1.64 (m, 14H). ^{13}C NMR (125 MHz, $CDCl_3$): δ = 129.62 (s, 1C, NCS), 62.17 (s, 1C, CH-NCS), 38.98 (s, 1C, Ad), 36.15 (s, 2C, Ad), 33.63 (s, 1C, Ad), 31.61 (s, 3C, Ad), 26.92 (s, 1C, Ad), 26.60 (s, 1C, Ad). Elemental analysis: calculated for $C_{11}H_{15}NS$: C 68.35, H 7.82, N 7.26, S 16.57; found C 68.36, H 7.81, N 7.25, S 16.60.

1-Isothiocyanatomethyladamantane (3).

The general method above was used with 1-aminomethyladamantane to afford white solid (1.07 g, 85% yield), mp 67-68°C. MS (EI): m/z (%) = 207 (14) $[M]^+$, 135 (100) $[Ad]^+$. ^1H NMR (400 MHz, DMSO-d6): δ = 3.29 (s, 2H, CH_2), 1.95 (s, 3H, Ad), 1.61 (dd, J = 11.7 Hz, J = 39.6 Hz, 6H, Ad), 1.47 (d, J = 2.5 Hz, 6H, Ad). ^{13}C NMR (100 MHz, $CDCl_3$): δ =

128.95 (s, 1C, NCS), 56.68 (s, 1C, CH_2-NCS), 39.55 (s, 1C, Ad), 37.05 (s, 1C, Ad), 36.65 (s, 3C, Ad), 34.86 (s, 1C, Ad), 28.22 (s, 1C, Ad), 28.04 (s, 3C, Ad). Elemental analysis: calculated for $C_{12}H_{17}NS$: C 69.52, H 8.26, N 6.76, S 15.46; found C 69.55, H 8.25, N 6.74, S 15.46.

1-Isothiocyanato-1-(adamantan-1-yl)ethane (4).

The general method above was used with 1-amino-1-(adamantan-1-yl)ethane to afford dark brown liquid crystallizing on storage (1.02 g, 82% yield). MS (EI): m/z (%) = 221 (12) $[M]^+$, 163 (8) $[Ad\text{-}CH(CH_3)]^+$, 135 (100) $[Ad]^+$. ^1H NMR (500 MHz, $CDCl_3$): δ = 3.35 (q, J = 6.5 Hz, 1 H, CH), 2.03 (s, 3 H), 1.74–1.46 (m, 12 H), 1.27 (d, J = 6.5 Hz, 3 H, CH_3). ^{13}C NMR (125 MHz, $CDCl_3$): δ = 128.50 (s, NCS), 63.68 (s, 1 C, CH), 38.22 (s, 3 C, Ad), 36.90 (s, quaternary C in Ad), 36.72 (s, 3 C, Ad), 28.17 (s, 3 C, Ad), 15.13 (s, 1 C, CH_3). Elemental analysis calculated for $C_{13}H_{19}NS$: C, 70.54; H, 8.65; N, 6.32; S, 14.49; found: C, 70.51; H, 8.66; N, 6.31; S 14.46.

1-Isothiocyanato-2-(adamantan-1-yl)ethane (5).

The general method above was used with 1-amino-2-(adamantan-1-yl)ethane to afford yellow viscous liquid (1.06 g, 86% yield). MS (EI): m/z (%) = 221 (15) $[M]^+$, 135 (100) $[Ad]^+$. ^1H NMR (500 MHz, $CDCl_3$): δ = 3.51 (t, J = 7.5 Hz, 2 H, CH_2-NCS), 1.96 (s, 3 H), 1.67 (dd, J = 32.0, 12.0 Hz, 4 H), 1.54–1.49 (m, 10 H). ^{13}C NMR (125 MHz, $CDCl_3$): δ = 128.99 (s, 1 C, NCS), 43.89 (s, 1 C, $\underline{C}H_2$-NCS), 41.88 (s, 3 C, Ad), 40.19 (s, 1 C, Ad-CH_2), 36.79 (s, 3 C, Ad), 28.38 (s, 3 C, Ad), 27.54 (s, 1 C, quaternary C in Ad). Elemental analysis calculated for $C_{13}H_{19}NS$: C, 70.54; H, 8.65; N, 6.32; S, 14.49; found: C, 70.50; H, 8.66; N, 6.32; S, 14.46.

1-Isothiocyanato-3-(adamantan-1-yl)propane (6).

The general method above was used with 1-amino-3-(adamantan-1-yl)propane to afford brown oil (0.23 g, 82% yield). MS (EI): m/z (%) = 234 (51) $[M]^+$, 202 (26) $[M - S]^+$, 175 (1) $[M - HNCS]^+$, 135 (100) $[Ad]^+$. ^1H NMR (500 MHz, $CDCl_3$): δ = 3.47 (t, J = 6.5 Hz, 2 H, CH_2-NCS), 1.96 (s, 3 H), 1.72-1.61 (m, 8 H), 1.47 (s, 6 H), 1.13 (t, J = 8.0 Hz, 2 H, $C\underline{H}_2$-Ad). ^{13}C NMR (125 MHz, $CDCl_3$): δ = 129.50 (s, 1 C, NCS), 45.99 (s, 1 C, $\underline{C}H_2$-NCS), 42.31 (s, 3 C, Ad), 41.33 (s, 1 C, Ad-CH_2), 37.09 (s, 3 C, Ad), 28.62 (s, 3 C, Ad), 28.43 (s, 1 C, Ad-$\underline{C}H_2$-CH_2-CH_2-NCS), 23.65 (s, 1 C, quaternary C in Ad). Elemental analysis calculated for $C_{14}H_{21}NS$: C, 71.44; H, 8.99; N, 5.95; S, 13.62; found: C, 71.45; H, 9.01; N, 5.93; S, 13.61.

1-(4-Isothiocyanatophenyl)adamantane (7).

The general method above was used with 4-(adamantan-1-yl)aniline to afford light brown solid (1.02 g, 82% yield), mp 120-121°C. MS (EI): m/z (%) = 269 (100) $[M]^+$, 212 (80) $[Ad\text{-}C_6H_4]^+$, 135 (4) $[Ad]^+$. ^1H NMR (500 MHz, $CDCl_3$): δ = 7.37 dd (4H, H_{arom}, J = 8.5, 36.8 Hz), 2.04 (3H, Ad), 1.82 s (6H, Ad), 1.72 s (6H, Ad). ^{13}C NMR (125 MHz, $CDCl_3$): δ = 150.95 (C_{arom}), 133.50 (NCS), 126.26 (4C, Carom), 125.52 (C_{arom}), 42.43 (3C, Ad), 36.14 (4C, Ad), 28.34 (3C, Ad). Elemental analysis calculated for $C_{17}H_{19}NS$: C, 75.79; H, 7.11; N, 5.20; S, 11.90; found: C, 75.77; H, 7.12; N, 5.25; S, 11.86.

1-(2-Isothiocyanatoethoxy)adamantane (8).

The general method above was used with 1-(2-aminoethoxy)adamantane to afford orange viscous liquid (0.78 g, 86% yield). MS (EI): m/z (%) = 237 (7) $[M]^+$, 151 (16) $[Ad\text{-}O]^+$, 135 (100) $[Ad]^+$. Elemental analysis calculated for $C_{13}H_{19}NOS$: C, 65.78; H, 8.07; N, 5.90; S, 13.51; found: C, 65.80; H, 8.04; N, 5.88; S, 13.55.

1-(2-Isothiocyanato-2-methylpropoxy)adamantane (9).

The general method above was used with 1-(adamantan-1-yloxy)-2-methylpropan-2-amine to afford orange viscous liquid (0.95 g, 80% yield). MS (EI): m/z (%) = 265 (10) $[M]^+$, 235 (75) $[M - 2CH_3]^+$, 135 (100) $[Ad]^+$. Elemental analysis calculated for $C_{15}H_{23}NOS$: C, 67.88; H, 8.73; N, 5.28; S, 12.08; found: C, 67.82; H, 8.72; N, 5.31; S, 12.11.

2-(1-Isothiocyanatopentan-2-yl)adamantane (10).

The general method above was used with 2-(adamantan-2-yl)pentan-1-amine to afford orange viscous liquid (1.06 g, 85% yield). MS (EI): m/z (%) = 263 (25) $[M]^+$, 262 (100) $[M - 1]^+$, 220 (60) $[M - CS]^+$, 135 (85) $[Ad]^+$. Elemental analysis calculated for $C_{16}H_{25}NS$: C, 72.95; H, 9.57; N, 5.32; S, 12.17; found: C, 72.96; H, 9.55; N, 5.31; S, 12.19.

1-Isothiocyanato-3,5-dimethyladamantane (11).

The general method above was used with 1-amino-3,5-dimethyladamantane to afford light orange viscous liquid (1.07 g, 86% yield). MS (EI): m/z (%) = 221 (5) $[M]^+$, 163 (100) $[Ad]^+$. ^1H NMR (500 MHz, $CDCl_3$): δ = 2.17 (s, 1 H), 1.81 (s, 2 H), 1.62 (dd, J = 13.0, 12.0 Hz, 4 H), 1.32 (dd, J = 16.0, 12.5 Hz, 4 H), 1.15 (s, 2 H), 0.87 (s, 6 H). ^{13}C NMR (125 MHz, $CDCl_3$): δ = 129.92 (s, 1 C, NCS), 59.75 (s, 1 C, C-NCS), 49.88 (s, 1 C, Ad), 49.61 (s, 2 C, Ad), 42.26 (s, 1 C, Ad), 41.89 (s, 2 C, Ad), 32.58 (s, 1 C, Ad), 29.90 (s, 2 C, Ad), 29.62 (s, 2 C, $2CH_3$). Elemental analysis calculated for $C_{13}H_{19}NS$: C, 70.54; H, 8.65; N, 6.30; S, 14.50; found: C, 70.59; H, 8.67; N, 6.27; S, 14.46.

Preparation of 2-(Adamantan-1-yl)acetyl isothiocyanate (12).

Ammonium thiocyanate (1.8 g, 23.5 mmol) was added to the solution of (adamantant-1-yl)acetic acid chloride (5 g, 23.5 mmol) in 50 mL of anhydrous acetone. After stirring for 1h at RT, ammonium chloride was filtered off and solvent was removed *in vacuo*. The residue was purified by crystallization from ethanol to afford yellow solid (5.24 g, 95%), mp 38-40°C. MS (EI): m/z (%) = 235 (40) $[M]^+$, 135 (100) $[Ad]^+$. Elemental analysis calculated for $C_{13}H_{17}NOS$: C 66.35; H 7.28; N 5.95; S 13.62; found: C 66.37; H 7.30; N 5.91; S 13.60.

Preparation of 3-(2-(Adamantan-1-yl)ethyl)-2-thioxoimidazolidin-4-one (13).

To a solution of compound **5** (1.0 g, 4.52 mmol) in DMF (8 mL), glycine ethyl ester hydrochloride (0.63 g, 4.52 mmol) and Et_3N (0.92 g, 9.04 mmol) were added. The mixture was stirred for 8h at RT. Solvent was removed *in vacuo*, and the crude product was crystallized from ethanol. Yield 0.94 g (75%), mp 180-181°C. For details, see Ref 28. MS (EI): m/z (%) = 278 (4) $[M]^+$, 245 (100) $[M - S]^+$, 143 (15%) [M – Ad], 135 (12) $[Ad]^+$, 117 (35) $[M - AdCH_2CH_2]$. ^1H NMR (500 MHz, $CDCl_3$): δ = 10.10 s (1H, NH), 4.09 s (2H, NH-C$\underline{H}_2$), 3.69-3.64 m (2H, N-C$\underline{H}_2$), 1.92 s (3H, Ad), 1.68-1.48 m (12H, Ad), 1.31-1.26

m (2H, Ad-C_H2). ^{13}C NMR (125 MHz, $CDCl_3$): δ = 183.13 (1C, C=S), 172.36 (1C, C=O), 76.55 (1C, NH-$\underline{C}H_2$-CH_2), 41.45 (3C, Ad), 40.85 (1C, N-CH_2), 36.41 (3C, Ad), 35.24 (1C, NH-CH_2-$\underline{C}H_2$), 31.35 (1C, Ad quart.), 27.83 (3C, Ad). Elemental analysis calculated for $C_{15}H_{22}N_2OS$: C 64.71; H 7.96; N 10.06; S 11.52; found: C 64.68; H 7.99; N 10.02; S 11.48.

Preparation of 1-Isoselenocyanato-2-(adamantan-1-yl)ethane (14).

$CHCl_3$ (1.5 mL), Aliquat 336 (0.15 g), and 50% aqueous NaOH (4 mL) were added to the solution of 2.0 g (11.17 mmol) 2-(adamantan-1-yl)ethylamine in 20 mL of CH_2Cl_2. After refluxing for 4h, selenium (Se) (5.0 g, 63.3 mmol) was added. After refluxing for another 4h, the mixture was cooled to RT and quenched with 30 mL of CH_2Cl_2 and 30mL of water. Excessive Se was filtered off, and organic layer was separated and dried with Na_2SO_4. After filtering the Na_2SO_4, solvent was removed *in vacuo*. The residue was purified by column chromatography (hexanes) to afford pale yellow solid (1.65 g, 55%), mp 78-79°C. For details, see Ref 28. MS (EI): m/z (%) = 269 (40) $[M]^+$, 188 (20) $[M - Se]^+$, 163 (70%) $[Ad\text{-}CH_2\text{-}CH_2]^+$, 149 (3%) $[Ad\text{-}CH_2]^+$, 135 (100) $[Ad]^+$. ^{1}H NMR (500 MHz, $CDCl_3$): δ = 3.60 t (2H, J = 8.0 Hz, $C\underline{H}_2$-NCSe), 1.98 s (3H, Ad), 1.61-1.73 m (6H, Ad), 1.56 t (2H, J = 8.0 Hz, Ad-$C\underline{H}_2$), 1.49 s (6H, Ad). Elemental analysis calculated for $C_{13}H_{19}NSe$: C 58.21; H 7.14; N 5.22; found: C 58.18; H 7.16; N 5.25.

Log *P* determination.

Each compound (10 μL of 10 mM solution in DMSO) was added to 0.5 mL of octanol and 0.5 mL of sodium phosphate buffer (pH 7.4) in 2 mL vial, stirred for 18h, and centrifuged for 2h at 3600 rpm as described previously[51]. Agilent LC 1200 MS 6420 triple quadrupole, column Zorbax xdb-c18 (Length 50 mm, diameter 2.1 mm, solid phase size 3.5 μm) was used to determine concentration in each phase.

Cell lines.

MDA-MB-231, MDA-MB-468, MDA-MB-436, HCC1937, and WT p53 MCF-7 cells were obtained from Tissue Culture Source Resource, Georgetown University, Washington, DC. MDA-MB-231, MDA-MB-468, and MCF-7 cells were cultured in Roswell Park Memorial Institute (RPMI) 1640 medium with 10% fetal bovine serum (FBS), 1% penicillin/streptomycin, and 1% L-glutamine. MDA-MB-436 were cultured in Dulbecco's Modified Eagle Medium (DMEM) medium with 10% FBS, 1% penicillin/streptomycin, and 1% L-glutamine. HCC1937 cells were cultured in RPMI 1640 medium with 10% FBS, 1% penicillin/streptomycin, 1% L-glutamine, and 1% sodium pyruvate. All the cell lines were negative for mycoplasma.

Cell proliferation assays.

The effect of different Ad-ITCs, PEITC, or adamantane on MDA-MB-231 cell proliferation was determined by using the WST-1 assay (Roche) as described previously (22,23). Briefly, each Ad-ITC was diluted in DMSO so that 10 μl of diluted stock in a 1 ml aliquot of cells (40,000 cells /ml) yielded a desired concentration at 1% DMSO. MDA-MB-231 cell cultures containing Ad-ITC were plated onto a 96-well micro titer plate at 4,000 cells per well in duplicate. As a control, 4,000 cells per well were seeded in medium containing 1%

DMSO in duplicate. For background subtraction, wells lacking cells but containing medium were used. Plates were incubated at 37 °C for 24 h or 72 h, followed by the addition of WST-1 reagent for 2 h. OD_{450} was measured using a microplate reader (Bio-Rad). Percent cell proliferation was calculated as the ratio of OD_{450} values obtained for respective cells grown in the presence of Ad-ITC compared with the presence of DMSO. Similar assays were performed to determine the effect of different Ad-ITCs, PEITC, or adamantane on proliferation of other cell lines.

Colony formation Assays.

To measure colony survival, 500 MDA-MB-231 or MCF-7 cells per well were seeded in a six-well plate 24 h before treatment. Cells then were treated with the indicated concentrations of different Ad-ITCs, Ad-ISeC **14**, or DMSO as a control for 24 h at 37 °C. Following treatment, cells were incubated in a regular medium (RPMI, 10% FBS) at 37 °C for 10 days. Colonies formed were fixed in methanol, stained with methylene blue (Sigma), and counted to determine percentage survival relative to the DMSO control.

Annexin V staining.

Annexin V staining was done in accordance with the manufacturer's instructions (Biolegend). In brief, cells were treated with Ad-ITCs **1**, **3**, **5**, **6**, Ad-compound **13**, or Ad-ISeC **14** or PEITC as indicated or DMSO as a control for 24 h. Cells were harvested by scraping, washed once with 1 x PBS, and resuspended in 0.5 ml Annexin V binding buffer. Cells were collected by centrifugation, 5 μl of the fluorochrome conjugated Annexin V was added in the residual buffer, and cells were incubated at RT in the dark for 15 min followed by the addition of 0.5 ml of Annexin V binding buffer and 5 μl of PI staining solution (0.1 μg/ml). Cells were then analyzed by flow cytometry using a BD LSRFORTESSA instrument (BD Biosciences).

Lysate preparation and western blot analysis.

Cells were treated with Ad-ITCs **1**, **3**, **5**, **6**, Ad-compound **13**, or Ad-ISeC **14** or PEITC as indicated or DMSO for 24 h. Cells were then harvested by centrifugation at 1600 × g for 10 min at 4 °C, washed once with PBS, resuspended in lysis buffer (20 mM Tris-Cl (pH 8.0), 137 mM sodium chloride, 10% glycerol, 1% NP-40, 2 mM EDTA) containing protease inhibitors cocktail (Roche Molecular Biochemicals), and were then incubated on ice for 30 min. The lysates were centrifuged at 18,500 × g for 10 min at 4 °C. Then 20 μg (MDA-MB-231 or MDA-MB-468) or 50 μg (MCF-7) of the lysates were loaded on 4-12% SDS-PAGE. Protein was transferred onto a PVDF membrane, and the blots were developed using the ECL Prime Western Blot Detection Kit according to the manufacturer's protocol (Amersham). The antibodies for p53 (DO-1) and GAPDH were purchased from Santa Cruz Biotechnology and Novus Biologicals, respectively.

Cells were treated with DMSO or 6 μM Ad-ITC **6** for 24 h. For detecting phosphorylation of ATM, 250 μg of the cell lysate was loaded on 4-12% SDS-PAGE. The proteins were then transferred onto a PVDF membrane, and blot was probed with anti-pATM Ser1981 antibody (1:500) (Santa Cruz Biotechnology). For the secondary antibody, peroxidase-labeled anti-mouse IgG (1:1000, GE Healthcare) was used. The blot was developed using the ECL

Prime Western Blot Detection Kit following the manufacturer's protocol (Amersham). As a control, the blot was probed with anti- GAPDH antibody (1: 5000) (Novus Biologicals).

Cells were treated with DMSO or Ad-ITC **6**, Ad-ISeC **14**, or PEITC at the indicated concentrations for 24 h. For detecting uncleaved caspase 3, uncleaved PARP1, or cleaved PARP1, 100 μg of the cell lysate was loaded on 4-12% SDS-PAGE. The proteins were then transferred onto a PVDF membrane, and blot was probed with anti-PARP (1:1000, BioLegend) or anti-caspase 3 (1:1000, Cell Signaling) antibodies. For the secondary antibody, peroxidase-labeled anti-mouse IgG (1:1000, GE Healthcare) or anti-rabbit (1:1000, Santa Cruz) was used. The blot was developed using the ECL Prime Western Blot Detection Kit following the manufacturer's protocol (Amersham). As a control, the blot was probed with anti- GAPDH antibody (1: 5000, Santa Cruz).

Real time polymerase chain reaction (qRT-PCR) assay.

Cells were treated with DMSO or 6 μM Ad-ITC **6** or Ad-ISeC **14** for 4 h. RNA was extracted using a Qiagen RNeasy Kit (Qiagen, Valencia, CA, USA), cDNA was synthesized by using High Capacity RNA to cDNA kit (Applied Biosystems, Invitrogen, Thermofisher Scientific), and the gene expression level was measured by qRT-PCR using TaqMan gene expression assays (Applied Biosystems, Invitrogen). The gene expression level was normalized with GAPDH, and the average is presented with standard deviation from triplicates of repeated experiments.

Flow-cytometric analysis.

Cells were treated with DMSO or 6 μM Ad-ITC **6** for 24 h. Cells were then prepared for flow cytometric analysis. Briefly, cells were washed with PBS free of Ca^{2+} and Mg^{2+}, trypsinized for 5 min, and harvested by centrifugation at 190 x g for 3 min at 4 °C. Cells were washed once with PBS, and pellets were resuspended in 1 ml of 70% ethanol and stored at −20°C overnight. Cells were harvested by centrifugation at 420 x g for 10 min. The cell pellets were washed once with 1 ml cold PBS and resuspended in 1 ml freshly prepared PI staining solution (PBS with 0.1% Triton X-100, 0.05 μg/ml propidium iodide, 0.1 mg/ml RNase (Sigma)). The cell suspension was incubated at room temperature for 30 min the in dark followed by incubation for 30 min at 4 °C. The samples were run on a Becton Dickinson FACS sort, and the data was analyzed using Mod Fit program (Verity Software House).

siRNA transfection in cells.

The p53 siRNA was obtained from SMARTpool (Thermo Scientific/Dharmacon, Lafayette, CO, USA). The siRNA was transfected using Lipofectamine 2000 as described previously (22,23). Briefly, MDA-MB-468 cells were plated to 50-60% confluence in 10 cm dishes 24 h before transfection. The siRNA (0.430 nmol) was mixed with 43 μl of Lipofectamine 2000 in 1 ml of Opti-MEM (Invitrogen). The mixture was added to the cells that subsequently were incubated for 5 h. After 24 h, a second transfection was performed similarly. Seventy-two hours after the initial transfection, cells were treated with Ad-ITC **6** or DMSO at the indicated concentrations, and cell proliferation was measured by using the WST-1 reagent (Sigma) as described previously.

Statistical Analysis.

Statistical differences in canonical p53 targets were evaluated with a two-tailed Student's *t* test. Differences were considered statistically significant at *p* values of ≤ 0.05. All statistical tests were two-sided.

Supplementary Material

Refer to Web version on PubMed Central for supplementary material.

Acknowledgements:

We thank Karen Creswell for Flow Cytometry at Georgetown University. We thank Tissue Culture Shared Resource (TCSR) at Georgetown University for the cell lines and the mycoplasma testing of these cell lines. Synthesis of isothiocyanates **1**-**12** is supported by grant of the Russian Science Foundation (project no. 19-73-10002), synthesis of isoselenocyanate **14** is supported by grant of the Russian Fund for Basic Research (project no. 20-03-00298). Mechanistic studies are supported by grant from National Cancer Institute of the National Institutes of Health (NIH) CA100853 and Lombardi Cancer Center Support Grant P30 CA51008.

Abbreviations used

Ad-ISeC	1-isoselenocyanato-2-(adamantan-1-yl)ethane
Ad-ITC	adamantyl isothiocyanate
ATM	Ataxia-Telangiectasia Mutated
CFA	colony formation assay
DDR	DNA damage response
DMEM	Dulbecco's Modified eagle Medium
DMSO	Dimethyl Sulfoxide
ER	estrogen receptor
FBS	fetal bovine serum
GOF	gain of function
HER2	human epidermal growth factor receptor 2
ITCs	isothiocyanates
NS	non-specific
PEITC	phenethyl isothiocyanate
PR	progesterone receptor
RPMI	Roswell Park Memorial Institute
RT-PCR	Real Time Polymerase Chain Reaction
S	sulfur

SARs	structure-activity relationships
SD	standard deviation
Se	selenium
TNBC	triple negative breast cancer
WT	wild-type

References

1. Gerzon K; Krumalns EV; Brindle RL; Marshall FJ; Root MA The adamantyl group in medicinal agents. I. Hypoglycemic N-Arylsulfonyl-N'-adamantylureas. J Med Chem. 1963, 6, 760–763. [PubMed: 14184942]
2. Rapala RT; Kraay RJ; Gerzon K The adamantyl group in medicinal agents. II. Anabolic steroid 17β-adamantoates. JMed Chem. 1965, 8, 580–583. [PubMed: 5867938]
3. Gerzon K; Kau D The adamantyl group in medicinal agents. III. Nucleoside 5′-adamantoates. The adamantoyl function as a protecting group. J Med Chem. 1967, 10, 189–199. [PubMed: 4167033]
4. Wanka L; Iqbal K; Schreiner PR The lipophilic bullet hits the targets: medicinal chemistry of adamantane derivatives. Chem Rev. 2013, 113, 3516–3604. [PubMed: 23432396]
5. Cady SD; Schmidt-Rohr K; Wang J; Soto CS; Degrado WF; Hong M Structure of the amantadine binding site of influenza M2 proton channels in lipid bilayers. Nature. 2010, 463, 689–692. [PubMed: 20130653]
6. Kozubik A; Horvath V; Svihalkova-Sindlerova L; Soucek K; Hofmanova J; Sova P; Kroutil A; Zak F; Mistr A; Turanek J High effectiveness of platinum(IV) complex with adamantylamine in overcoming resistance to cisplatin and suppressing proliferation of ovarian cancer cells in vitro. Biochem Pharmacol. 2005, 69, 373–383. [PubMed: 15652229]
7. Blanařova OV; Safařikova B; Herůdkova J; Krkoska M; Tomankova S; Kahounova Z; Andera L; Bouchal J; Kharaishvili G; Krai M; Sova P; Kozubik A; Vaculova AH Cisplatin or LA-12 enhance killing effects of TRAIL in prostate cancer cells through Bid-dependent stimulation of mitochondrial apoptotic pathway but not caspase-10. PloS one. 2017, 12, e0188584. [PubMed: 29182622]
8. Herůdková J; Paruch K; Khirsariya P; Souček K; Krkoška M; Blanářová OV; Sova P; Kozubik A; Vaculova AH CHK1 inhibitor SCH900776 effectively potentiates the cytotoxic effects of platinum-based chemotherapeutic drugs in human colon cancer cells. Neoplasia. 2017, 19, 830–841. [PubMed: 28888100]
9. Prochazka L; Turanek J; Tesarik R; Knotigova P; Polaskova P; Andrysik Z; Kozubik A; Zak F; Sova P; Neuzil J; Machala M Apoptosis and inhibition of gap-junctional intercellular communication induced by LA-12, a novel hydrophobic platinum(IV) complex. Arch Biochem Biophys. 2007, 462, 54–61. [PubMed: 17466256]
10. Zefirov NA; Hoppe M; Kuznetsova IV; Chernyshov NA; Grishin YK; Maloshitskaya OA; Kuznetsov SA; Zefirova ON Homologous series of novel adamantane–colchicine conjugates: synthesis and cytotoxic effect on human cancer cells. Mendeleev Communications. 2018, 28, 308–310.
11. Vasilenko DA; Dueva EV; Kozlovskaya LI; Zefirov NA; Grishin YK; Butov GM; Palyulin VA; Kuznetsova TS; Karganova GG; Zefirova ON; Osolodkin DI; Averina EB Tick-borne flavivirus reproduction inhibitors based on isoxazole core linked with adamantane. Bioorganic Chem. 2019, 87, 629–637.
12. Svingen PA; Tefferi A; Kottke TJ; Kaur G; Narayanan VL; Sausville EA; Kaufmann SH Effects of the Bcr/Abl kinase inhibitors AG957 and NSC 680410 on chronic myelogenous leukemia cells in vitro. Clin Can Res. 2000, 6, 237–249.
13. Conaway CC; Yang YM; Chung FL Isothiocyanates as cancer chemopreventive agents: their biological activities and metabolism in rodents and humans. Curr Drug Metab. 2002, 3, 233–255. [PubMed: 12083319]

14. Talalay P; Fahey JW Phytochemicals from cruciferous plants protect against cancer by modulating carcinogen metabolism. J Nutr. 2001, 131, 3027S–3033S. [PubMed: 11694642]
15. WHOIARC handbook on cancer prevention. Cruciferous vegetables, isothiocyanates and indoles, vol. 9. (Lyon: IARC Press, 2004).
16. Huang C; Ma WY; Li J; Hecht SS; Dong Z Essential role of p53 in phenethyl isothiocyanate-induced apoptosis. Can Res. 1998, 58, 4102–4106.
17. Kensler TW; Egner PA; Agyeman AS; Visvanathan K; Groopman JD; Chen JG; Chen TY; Fahey JW Talalay P Keap1-nrf2 signaling: a target for cancer prevention by sulforaphane. Top Curr Chem. 2013, 329, 163–177. [PubMed: 22752583]
18. Kong AN; Owuor E; Yu R; Hebbar V; Chen C; Hu R; Mandlekar S Induction of xenobiotic enzymes by the MAP kinase pathway and the antioxidant or electrophile response element (ARE/EpRE). Drug Metab Rev. 2001, 33, 255–271. [PubMed: 11768769]
19. Xiao D; Lew KL; Zeng Y; Xiao H; Marynowski SW; Dhir R; Singh SS Phenethyl isothiocyanate-induced apoptosis in PC-3 human prostate cancer cells is mediated by reactive oxygen species-dependent disruption of the mitochondrial membrane potential. Carcinogenesis. 2006, 27, 2223–2234. [PubMed: 16774948]
20. Trachootham D; Zhou Y; Zhang H; Demizu Y; Chen Z; Pelicano H; Chiao PJ; Achanta G; Arlinghaus RB; Liu J; Huang P Selective killing of oncogenically transformed cells through a ROS-mediated mechanism by beta-phenylethyl isothiocyanate. Cancer Cell. 2006, 10, 241–252. [PubMed: 16959615]
21. Wang X; Di Pasqua AJ; Govind S; McCracken E; Hong C; Mi L; Mao Y; Wu JYC; Tomita Y; Woodrick JC; Fine RL; Chung F-L Selective depletion of mutant p53 by cancer chemopreventive isothiocyanates and their structure-activity relationships. J Med Chem. 2011, 54, 809–816. [PubMed: 21241062]
22. Aggarwal M; Saxena R; Sinclair E; Fu Y; Jacobs A; Dyba M; Wang X; Cruz I; Berry D; Kallakury B; Mueller SC; Agostino SD; Blandino G; Avantaggiati ML; Chung F-L. Reactivation of mutant p53 by a dietary-related compound phenethyl isothiocyanate inhibits tumor growth. Cell Death Differ. 2016, 23, 1615–1627. [PubMed: 27258787]
23. Aggarwal M; Saxena R; Asif N; Sinclair E; Tan J; Cruz I; Berry D; Kallakury B; Pham Q; Wang TTY; Chung F-L p53 mutant-type in human prostate cancer cells determines the sensitivity to phenethyl isothiocyanate induced growth inhibition. J Exp Clin Cancer Res. 2019, 38, 307–323. [PubMed: 31307507]
24. Walerych D; Napoli M; Collavin L; Sal GD The rebel angel: mutant p53 as the driving oncogene in breast cancer. Carcinogenesis. 2012, 33, 2007–2017. [PubMed: 22822097]
25. Blandino G; Di Agostino S New therapeutic strategies to treat human cancers expressing mutant p53 proteins. J Exp Clin Cancer Res. 2018, 37, 30–42. [PubMed: 29448954]
26. Shah SP; Roth A; Goya R; Oloumi A; Ha G; Zhao Y; Turashvili G; Ding J; Tse K; Haffari G; Bashashati A; Prentice LM; Khattra J; Burleigh A; Yap D; Bernard V; McPherson A; Shumansky K; Crisan A; Giuliany R; Heravi-Moussavi A; Rosner J; Lai D; Birol I; Varhol R; Tam A; Dhalla N; Zeng T; Ma K; Chan SK; Griffith M; Moradian A; Cheng S-WG; Morin GB; Watson P; Gelmon K; Chia S; Chin S-F; Curtis C; Rueda OM; Pharoah PD; Damaraju S; Mackey J; Hoon K; Harkins T; Tadigotla V; Sigaroudinia M; Gascard P; Tlsty T; Costello JF; Meyer IM; Eaves CJ; Wasserman WW; Jones S; Huntsman D; Hirst M; Caldas C; Marra MA; Aparicio S The clonal and mutational evolution spectrum of primary triple-negative breast cancers. Nature. 2012, 486, 395–399. [PubMed: 22495314]
27. Pitushkin DA; Burmistrov VV; Butov GM Synthesis of homologs of 1-isothiocyanatoadamantane. Russ J Org Chem. 2018, 54, 1475–1479.
28. Bumistrov VV; Pitushkin DA; Vasipov VV; D'yachenko VS; Butov GM Synthesis of 3-adamantylated hydantoins and their 2-thio(seleno) analogs. Chem Heterocycl Com. 2019, 55, 619–622.
29. Lipinski CA; Lombardo F; Dominy BW; Feeney PJ Experimental and computational approaches to estimate solubility and permeability in drug discovery and development settings. Adv Drug Deliv Rev. 2001, 46, 3–25. [PubMed: 11259830]

30. Cady SD; Wang J; Wu Y; DeGrado WF; Hong M Specific binding of adamantane drugs and direction of their polar amines in the pore of the influenza M2 transmembrane domain in lipid bilayers and dodecylphosphocholine micelles determined by NMR spectroscopy. J Am Chem Soc. 2011, 133, 4274–4284. [PubMed: 21381693]

31. Du QS; Wang SQ; Chen D; Meng JZ; Huang RB In depth analysis on the binding sites of adamantane derivatives in HCV (Hepatitis C Virus) p7 channel based on the NMR structure. PLoS One. 2014, 9, e93613. [PubMed: 24714586]

32. Morse MA; Eklind KI; Hecht SS; Jordan KG; Choi CI; Desai DH; Amin SG; Chung F-L Structure-activity relationships for inhibition of 4-(methylnitrosamino)-1-(3-pyridyl)-1-butanone lung tumorigenesis by arylalkyl isothiocyanates in A/J Mice. Cancer Res. 1991, 51, 1846–1850. [PubMed: 2004368]

33. Chaitanya GV; Alexander JS; Babu PP PARP-1 cleavage fragments: signatures of cell-death proteases in neurodegeneration. Cell Commun Signal. 2010, 8, 31–41. [PubMed: 21176168]

34. Jänicke RU; Ng P; Sprengart ML; Porter AG Caspase-3 is required for alpha-fodrin cleavage but dispensable for cleavage of other death substrates in apoptosis. J Biol Chem. 1998, 273, 15540–15545. [PubMed: 9624143]

35. Ryan KM; Phillips AC; Vousden KH Regulation and function of the p53 tumor suppressor protein. Curr Opin Cell Biol. 2001, 3, 332–337.

36. Liu DP; Song H; Xu Y A common gain of function of p53 cancer mutants in inducing genetic instability. Oncogene. 2010, 29, 949–956. [PubMed: 19881536]

37. Jackson M; Combs G Selenium and anticarcinogenesis: underlying mechanisms. Curr Opin Clin Nutr and Metab Care. 2008, 11, 718–726.

38. Brigelius-Flohé R; Banning A Part of the series: from dietary antioxidants to regulators in cellular signaling and gene regulation. Sulforaphane and selenium, partners in adaptive response and prevention of cancer. Free Radic Res. 2006, 40, 775–787. [PubMed: 17015256]

39. Zakrzewski J; Huras B; Kiełczewska A Synthesis of isoselenocyanates. Synthesis. 2016, 48, 85–96.

40. Dittmer D; Pati S; Zambetti G; Chu S; Teresky AK; Moore M; Finlay C; Levine AJ Gain of function mutations in p53. Nat Genet. 1993, 4, 42–46. [PubMed: 8099841]

41. Freed-Pastor WA; Prives C Mutant p53: one name, many proteins. Genes Dev. 2012, 26, 1268–1286. [PubMed: 22713868]

42. Bykov VJ; Issaeva N; Shilov A; Hultcrantz M; Pugacheva E; Chumakov P; Bergman J; Wiman KG; Selivanova S Restoration of the tumor suppressor function to mutant p53 by a low-molecular-weight compound. Nat Med. 2002, 8, 282–288. [PubMed: 11875500]

43. Yu X; Vazquez A; Levine AJ; Carpizo DR Allele-specific p53 mutant reactivation. Cancer Cell. 2012, 21, 614–625. [PubMed: 22624712]

44. Barrera LN; Cassidy A; Johnson IT; Bao Y; Belshaw NJ Epigenetic and antioxidant effects of dietary isothiocyanates and selenium: potential implications for cancer chemoprevention. ProcNutr Soc. 2012, 71, 237–245.

45. Sharma AK; Sharma A; Desai D; Madhunapantula SV; Huh SJ; Robertson GP; Amin S Synthesis and anticancer activity comparison of phenylalkyl isoselenocyanates with corresponding naturally occurring and synthetic isothiocyanates. J Med Chem. 2008, 51, 7820–7826. [PubMed: 19053750]

46. Westland RD; Merz MM; Alexander SM; Newton LS; Bauer L; Conway TT; Barton JM; Khullar KK; Devdhar PB; Grenan MM 2-Mercaptoacetamidine and derivatives as antiradiation agents. J Med Chem. 1972, 15(12), 1313–1321. [PubMed: 4635980]

47. Shirole NH; Pal D; Kastenhuber ER; Senturk S; Boroda J; Pisterzi P; Miller M; Munoz G; Anderluh M; Ladanyi M; Lowe SW; Sordella R TP53 exon-6 truncating mutations produce separation of function isoforms with pro-tumorigenic functions. eLife. 2016, 5, e17929. [PubMed: 27759562]

48. Liu MY; Meng SN; Wu HZ; Wang S; Wei MJ Pharmacokinetics of single-dose and multiple-dose memantine in healthy chinese volunteers using an analytic method of liquid chromatography-tandem mass spectrometry. Clin Ther. 2008, 30, 641–653. [PubMed: 18498913]

49. Hayden FG; Minocha A; Spyker DA; Hoffman HE Comparative single-dose pharmacokinetics of amantadine hydrochloride and rimantadine hydrochloride in young and elderly adults. Antimicrob Agents Chemother. 1985, 28(2), 216–221. [PubMed: 3834831]

50. Liebes L; Hochster H; Conaway CC; Chachoua A; Sewak S; Farrell K; Cosmidis A; Mendoza S; Shore R; Crowell J; Hecht SS; Carmella S; Chung F-LThirty day multiple dose administration of PEITC: A phase I study with steady state pharmacokinetics showing good tolerance through 120 mg daily. Proc Am Assoc Cancer Res. 2001, 42, 834.

51. Chiang PC; Hu Y Simultaneous determination of LogD, LogP, and pK(a) of drugs by using a reverse phase HPLC coupled with a 96-well plate auto injector. Comb Chem High Throughput Screen. 2009, 12, 250–257. [PubMed: 19275530]

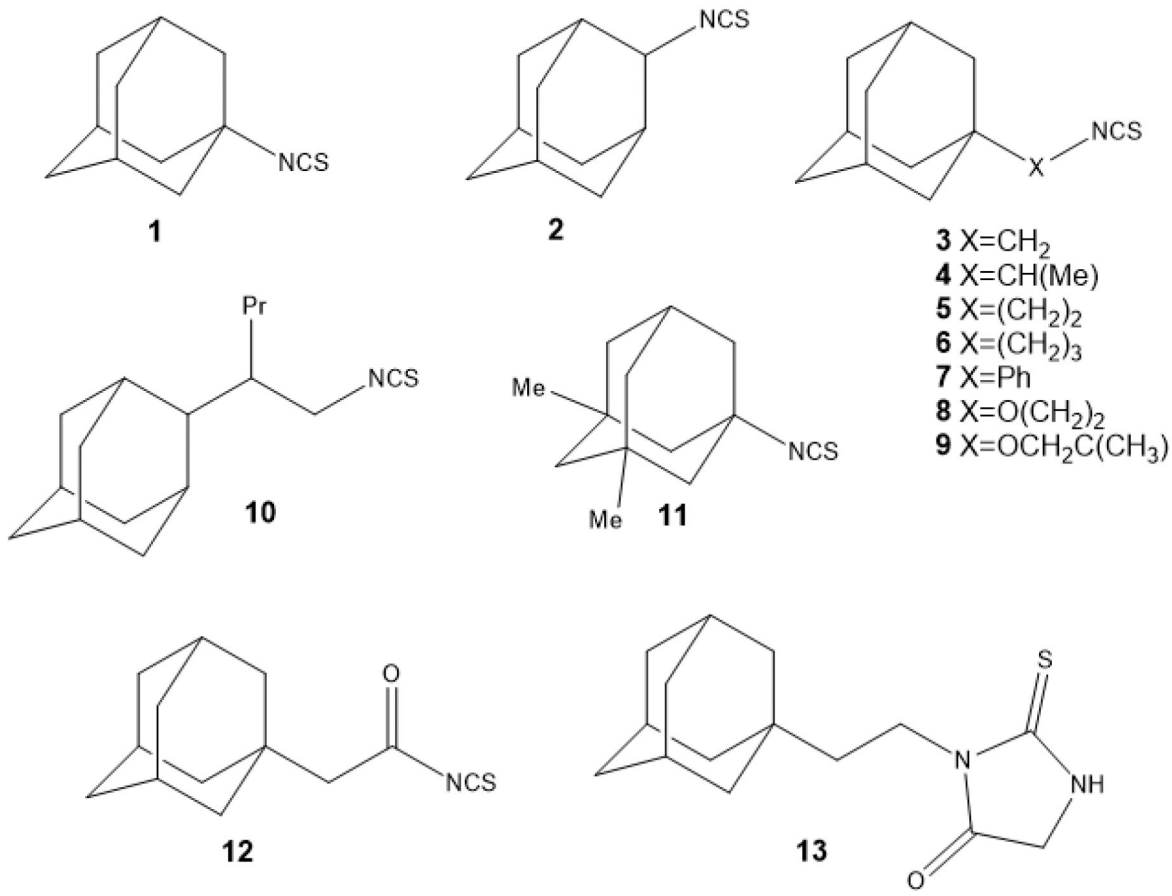

Figure 1. Structures of Ad-ITCs and Ad-compound 13.

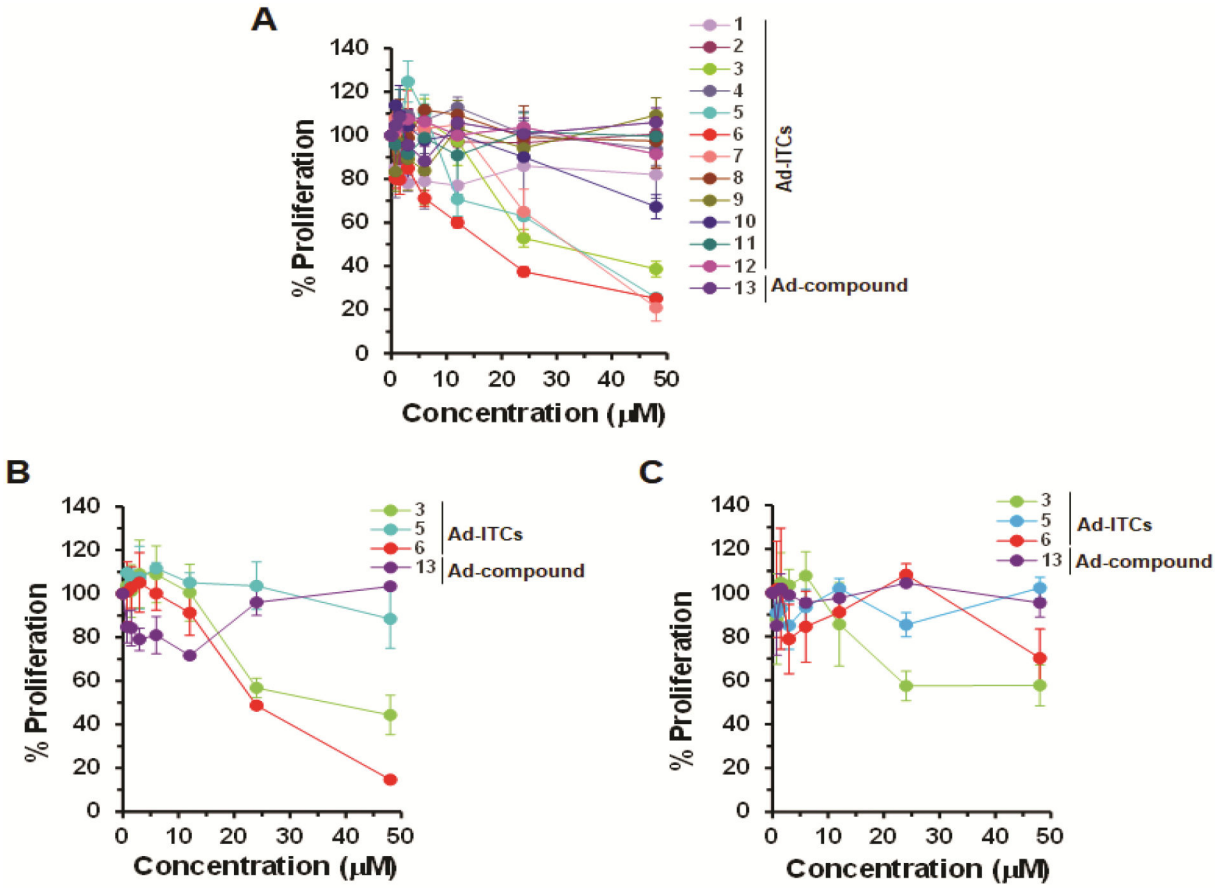

Figure 2. Effects of Ad-ITCs on the proliferation of breast cancer cell lines expressing mutant p53 or WT p53.

(**A-C**) The mutant p53 ($p53^{R280K}$ MDA-MB-231 and $p53^{R273H}$ MDA-MB-468) and WT p53 (MCF-7) cells, respectively, were treated with DMSO (as a control) or different Ad-ITCs or Ad-compound **13** at the indicated concentrations for 24 h. Percent cell proliferation determined by WST-1 was calculated as the ratio of OD_{450} values obtained for cells grown in the presence of the respective Ad-ITC or Ad-compound **13** compared with that of DMSO. Experiments were performed in triplicate. Error bars represents standard deviations (SD).

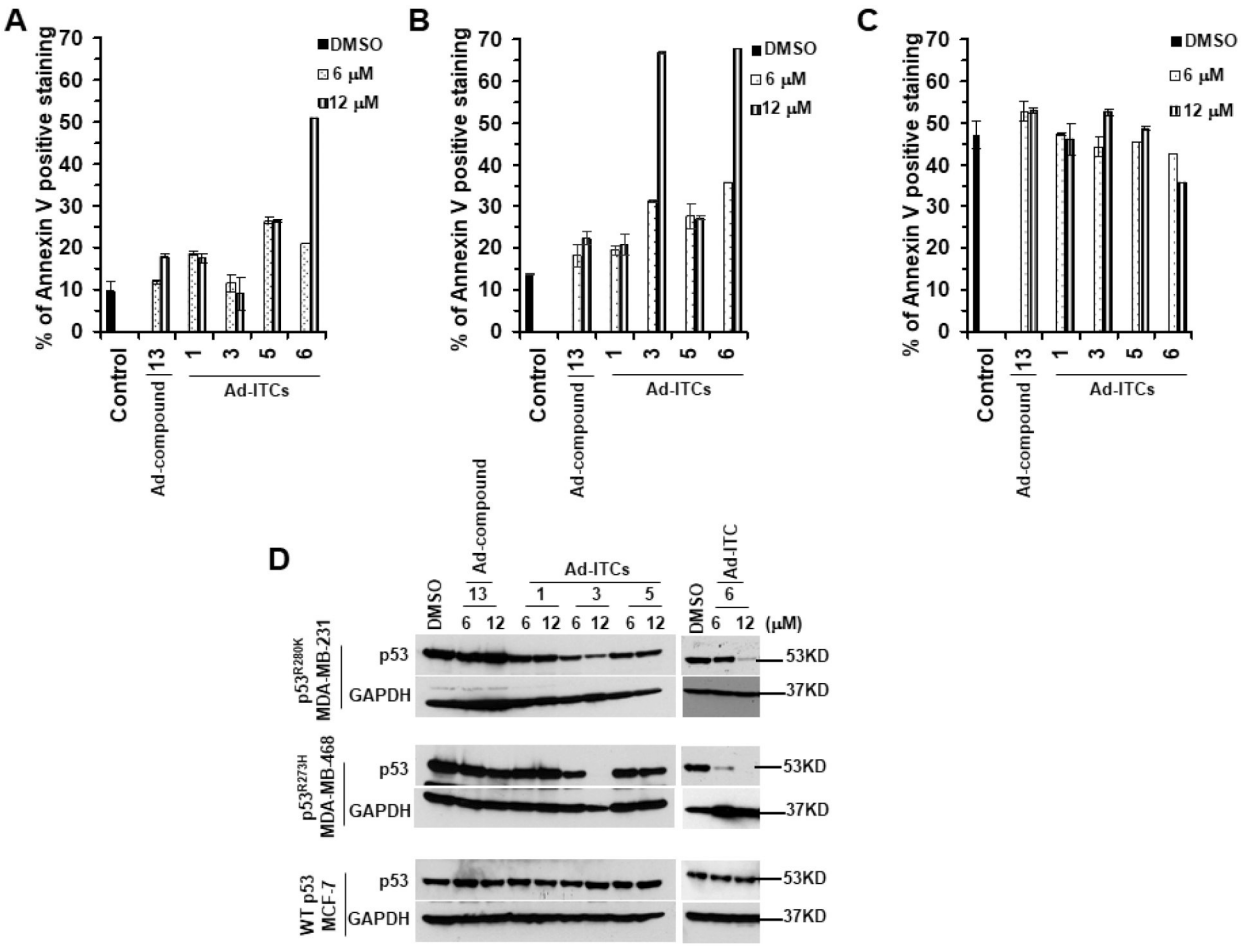

Figure 3. Effects of Ad-ITCs on apoptosis induction and p53 levels in breast cancer cell lines with mutant p53 or WT p53.

(**A-C)** The mutant p53 ($p53^{R280K}$ MDA-MB-231 and $p53^{R273H}$ MDA-MB-468) and WT p53 (MCF-7) cells, respectively, were treated with DMSO (as a control) or different Ad-ITCs or Ad-compound **13** at the indicated concentrations for 24 h. Apoptosis was measured by Annexin-V staining by flow cytometry using a BD LSRFORTESSA instrument. Percent of Annexin-V positive stained cells were calculated as the ratio of stained cells obtained for cells grown in the presence of the respective Ad-ITC or Ad-compound **13** compared with the presence of DMSO. (**D)** SARs for the depletion of mutant p53 levels by Ad-ITCs. The mutant p53 ($p53^{R280K}$ MDA-MB-231 and p53 ^{R273H} MDA-MB-468) and WT p53 (MCF-7) cells, respectively, were treated with DMSO (as a control) or 6 μM or 12 μM of different Ad-ITCs or Ad-compound **13** for 24 h. Cells were harvested and lysates were prepared. Twenty μg or 50 μg of the mutant p53 or WT p53 cell lysate fractions, respectively, were resolved by SDS-PAGE and probed with p53 DO-1 antibody. Blots were stripped and re-probed with anti-GAPDH as a loading control. Experiments were performed in triplicate. Error bars represents SD.

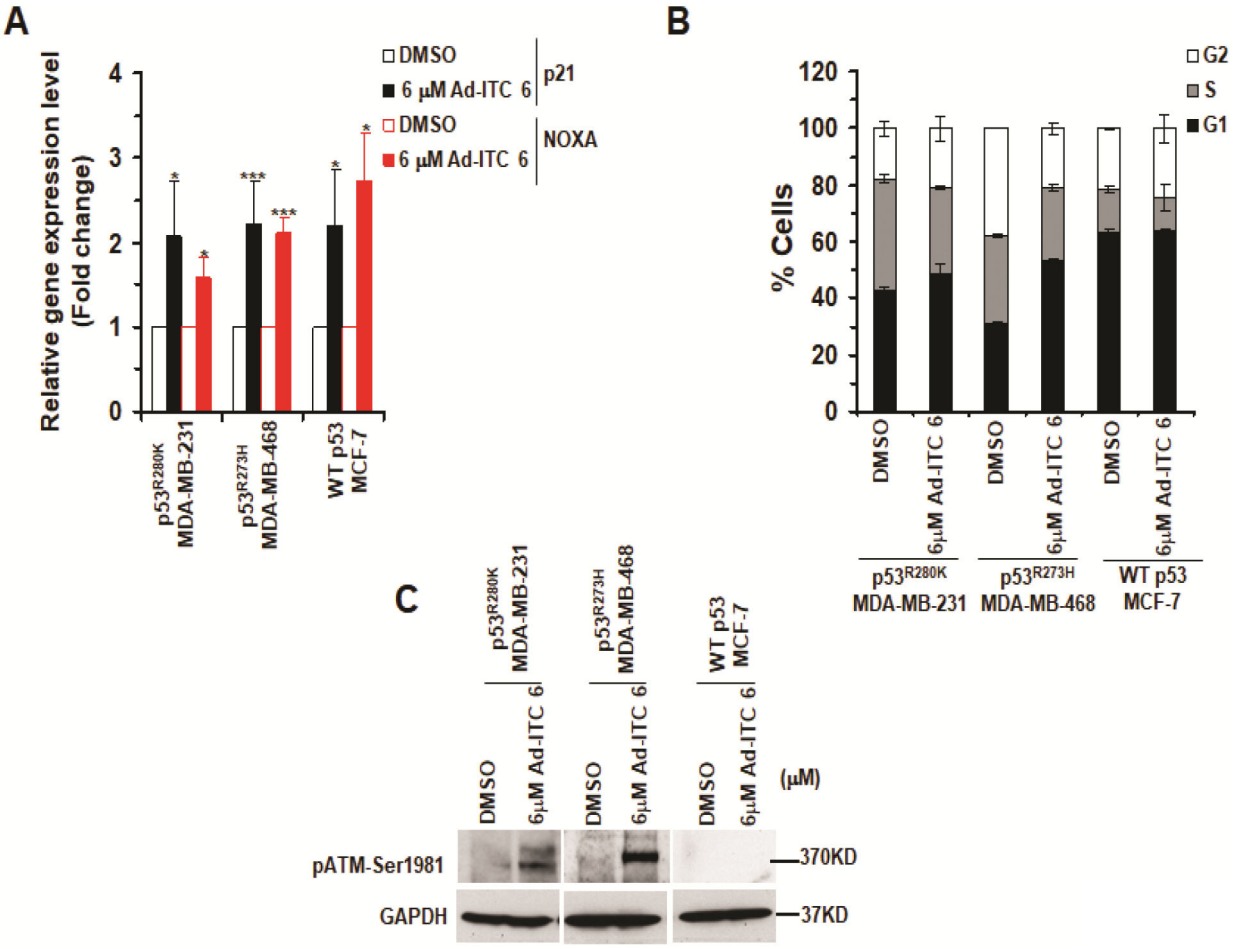

Figure 4. Effects of Ad-ITC 6 on canonical p53 targets, cell cycle progression, and activation of ATM.

(**A**) qRT-PCR of p53 regulated downstream target genes p21 and NOXA in mutant p53 ($p53^{R280K}$ MDA-MB-231, $p53^{R273H}$ MDA-MB-468) and WT p53 (MCF-7) cell treated with DMSO or 6 μM of Ad-ITC **6** for 4 h. (***p ≤ .0005 and *p ≤ 0.05). (**B)** Cells were treated with DMSO or 6 μM of Ad-ITC **6** for 24 h and analyzed by flow cytometry. (**C)** Cells were treated with DMSO or 6 μM of Ad-ITC **6** for 24 h. Blots were probed using anti-pATM S1981 antibody and reprobed with GAPDH antibody. Experiment were performed in triplicate. Error bars represents SD.

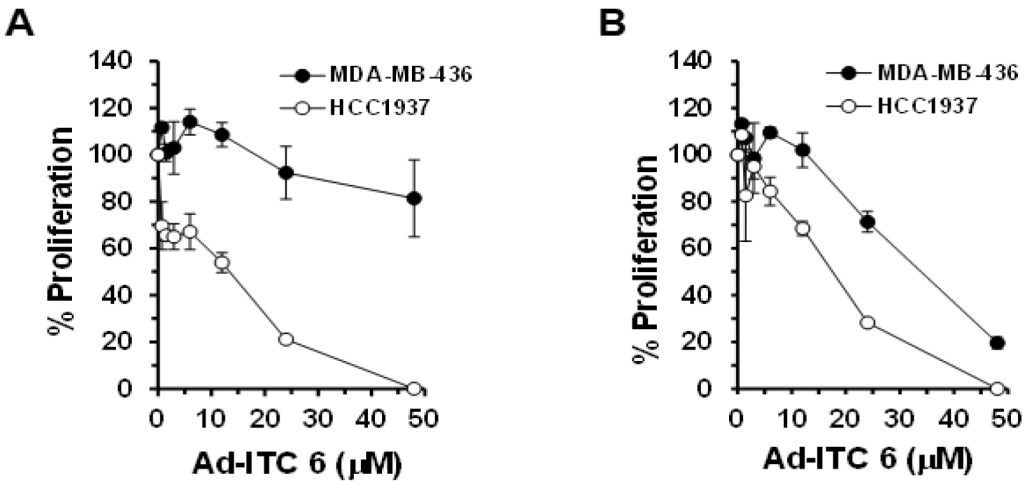

Figure 5. Effects of Ad-ITC 6 on the proliferation of MDA-MB-436 (p53 null) and HCC1937 (truncated mutant p53) cells.

Cells were treated with DMSO (as a control) or Ad-ITC **6** at the indicated concentrations for 24 h (**A**) or 72 h (**B**). Percent cell proliferation determined by WST-1 was calculated as the ratio of OD_{450} values obtained for cells grown in the presence of the Ad-ITC **6** compared with the presence of DMSO. Experiments were performed in triplicate. Error bars represents SD.

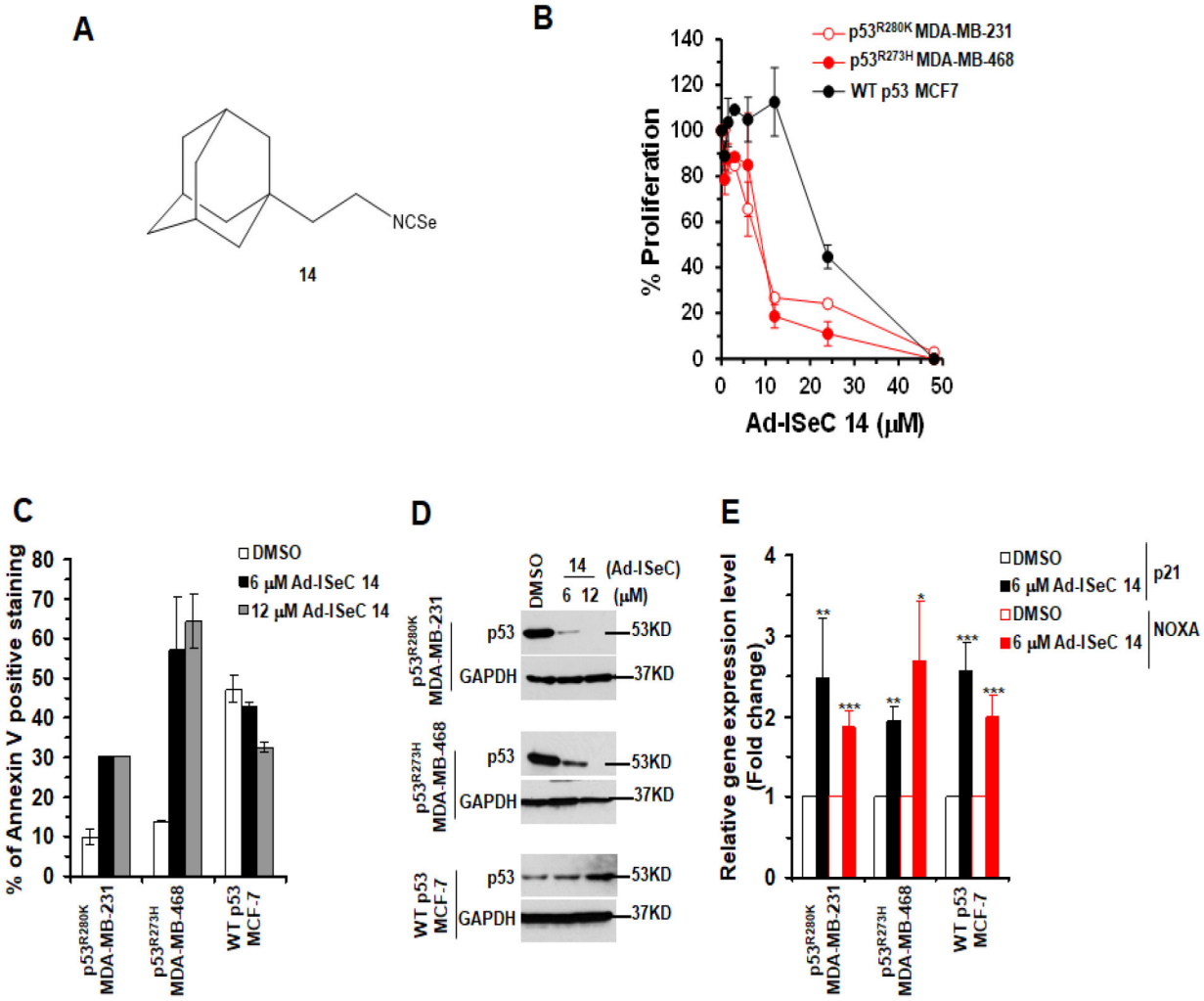

Figure 6. Ad-ISeC 14 showed an enhanced potency to inhibit the growth of TNBC with mutant p53.

(A) Structure of Ad-ISeC **14**. (**B**) The mutant p53 ($p53^{R280K}$ MDA-MB-231 and $p53^{R273H}$ MDA-MB-468) and WT p53 (MCF-7) cells, respectively, were treated with DMSO or Ad-ISeC **14** for 24 h. Percent cell proliferation determined by WST-1 was calculated as the ratio of OD_{450} obtained for cells grown in the presence of Ad-ISeC **14** compared with the presence of DMSO. (**C)** The mutant p53 and WT p53 cells were treated with DMSO or Ad-ISeC **14** for 24 h. Apoptosis was measured by Annexin-V staining. Percent of Annexin-V positive stained cells were calculated as the ratio of stained cells obtained for cells grown in the presence of the Ad-ISeC **14** compared with the presence of DMSO. (**D**) The mutant p53 and WT p53 cells were treated with DMSO or Ad-ISeC **14** (6 μM or 12 μM) for 24 h and mutant p53 expression was analyzed. Twenty or 50 μg of the mutant or WT p53 cell lysate fractions, respectively, were resolved by SDS-PAGE and probed with p53 DO-1 antibody. Blots were re-probed with anti-GAPDH as a loading control. (**E**) Effects of Ad-ISeC **14** on canonical p53 targets. qRT-PCR of p53 regulated downstream target genes p21 and NOXA in mutant p53 and WT p53 cell treated with DMSO or 6 μM Ad-ISeC **14**

for 4 h. (***p ≤ .0005, **p ≤ .005 and *p ≤ 0.05). Experiments were performed in triplicate. Error bars represents SD.